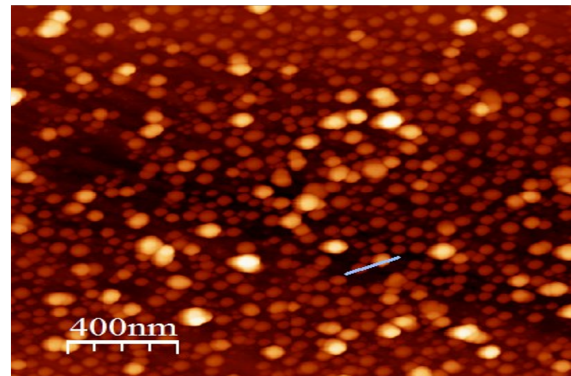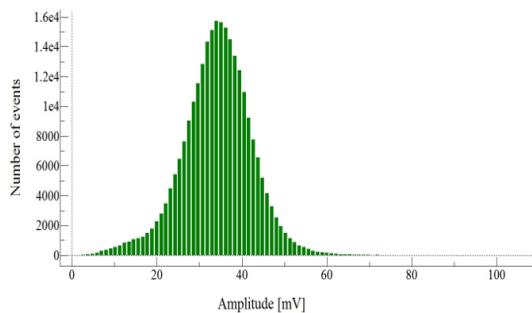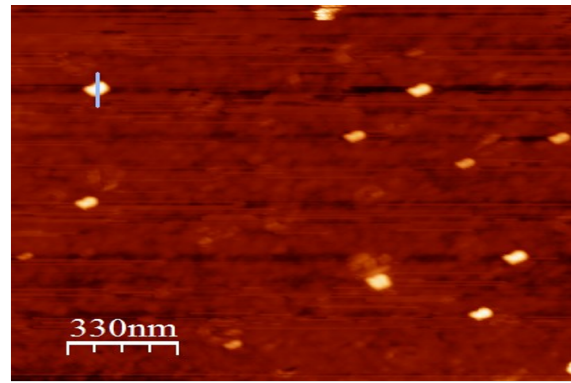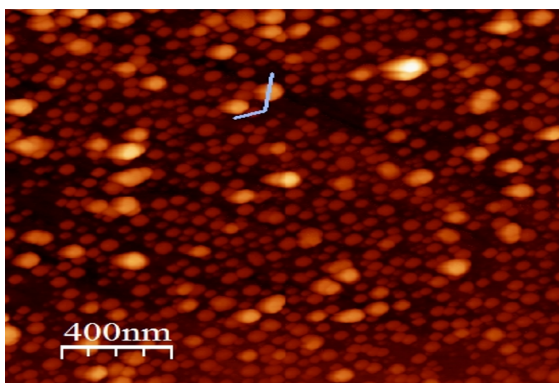AALBORG UNIVERSITY

DEPARTMENT OF PHYSICS AND NANOTECHNOLOGY

FORTH SEMESTER NANOBIOTECHNOLOGY PROJECT

SYNTHESIS OF SILVER NANOPARTICLE DIMERS

Authors:

Prerak PATEL

Supervisor:

Leonid GUREVICH

Co-Supervisor:

Peter FOJAN

AALBORG UNIVERSITET

June 20, 2019

Forth semester of master studies of Nanobiotechnology at School of Engineering and Science

The Faculty of Natural Sciences

Physics and Nanotechnology

Skjernvej 4a

9220 Aalborg Ø

Title:

SYNTHESIS OF SILVER NANOPARTICLE DIMERS

Project period:

February 2019 - June 2019

Author:

Prerak Patel

Supervisor:

Leonid Gurevich

Co-Supervisor:

Peter Fojan

Copies: 1

Total pages: 66

Appendices: 0

Finalized 19-06-2019

Abstract:

Nanoparticle dimers composed of two adjacent metal nanoparticles can amplify electromagnetic fields on nanoscale and hold a promise for developing of ultrasensitive biosensors. The focus of the project is on the preparation of dimers consisting of silver nanoparticles. The dimers will be prepared using a combination of silver nanoclusters produced by magnetron spattering (MaSCA) and deposited on a polymer coated solid substrate and colloidal silver nanoparticles produced in solution. The obtained nanoparticles and dimers will be studied using Atomic Force Microscopy, Scanning Electron Microscopy and UV-VIS absorption spectroscopy.

Prologue

The following project is written in the period from February the 15th,2019 to June the 20th, 2019 by an individual master nanobiotechnology student from Aalborg University with associate professor Leonid Gurevich acting as primary supervisor and associate professor Peter Fojan acting as a Co-supervisor In this report, Silver nanoparticle dimers have been successfully synthesized using Silver and copper clusters prepared by with cluster beam technique using Magnetron Sputtering Cluster Apparatus and Colloidal silver nanoparticles. The synthesized clusters, nanoparticles and dimers have been characterized by UV visible spectroscopy,Nanoparticle tracking analysis and Atomic force microscopy. Relevant theory and methodology about the project will be explained. Finally, the results obtained will be presented and discussed.

The experiments were done in biolab, Physics lab at Aalborg University Department of Physics and Nanotechnology.

The citations in this report will be placed before the dot if the citation relates the sentence e.g.: '[number].' , and after the dot if the citation relates to the paragraph e.g.: '.[number]'. Figures used in this report will be referenced as adopted if they are directly the same as the one cited to, or as adapted if it is inspired by the cited publication. If there is no citation for the figure, it is unique for this report.

_____
Prerak Patel

Contents

1. Introduction

Metal nanocrystals and nanostructures are promising materials for countless nanophotonic applications due to their strong interactions with light. Their optical properties are dominated by the localized surface plasmon resonances (LSPR), the collective coherent oscillation of conduction electrons in the metallic nanostructures. [1] [2] For a given type of noble metal, the resonance energy of the LSPR is highly sensitive to the size, morphology, and configuration of the nanostructures.[3] Among all types of complex nanostructures, pairs of nanocrystals are the simplest model system to study. The close approach of two nanocrystals leads to interaction of their LSPR, which further results in highly enhanced and localized plasmons or "hot spots" at the junctions between the nanocrystals. Hot spots give rise to large enhancements of the electromagnetic field locally, which enables molecular detection through surface-enhanced Raman scattering (SERS) at or near single molecule sensitivity.[4]

Nanocrystal pairs with an intra-particle distance smaller than the diameter of the nanocrystals are known as "dimers". Dimers can create extremely large plasmonic enhancements in their junctions and have been widely explored as SERS substrates.[5] Studies have revealed that, when the spacing between two nanocrystals is below 0.5 nm, especially with slight fusing of the nanocrystals within a dimer to give tiny crevices, the plasmonic electromagnetic enhancements could be 10^{10} times or greater.[6] Importantly, electromagnetic coupling of the plasmon resonance between two nanocrystals follows the principles of molecular hybridization. This means that, when very strong plasmonic enhancement is in place within a dimer, two nanocrystal plasmons hybridize to form a lower energy bonding plasmon mode and a higher energy antibonding plasmon mode.[7] This offers a convenient tool for characterization of the formation of dimers of noble metal nanocrystals. Thus, if high purity dimers are present in a sample, it should be possible to observe a two-band absorption spectrum for the sample, given that the size of the nanocrystals, the distance between the two nanocrystals, and the degree of fusion between the two nanocrystals are tightly controlled.

Bottom-up methods are commonly used to form plasmonic NP dimers or multimers, e.g., via complementary DNA[8] , click chemistry [9], Diels-Alder [10], and other chemical reactions as well as the formation of metal complexes [11]. It is also possible to use functionalized organic molecules in order to initialize the assembly process. These linker molecules comprise a multitude of different structures and functionalities like flexible dithiols or rigid molecules with a conjugated or metal complex backbone [12]. However, the exact bonding mode of these linkers remains an open question since contradictory

results have been reported in literature. A shift of the plasmon band over time during the NP assembly by a polyphenylene dendrimer linker was noted. This could indicate a transformation from assemblies of particles with the maximum possible distance to assemblies with distances shorter than the length of the linker [13] .

Moreover, once being fabricated, it remains challenging to measure the optical properties of an isolated NP or dimer, or even just finding its exact position on a substrate without destroying the sample. But the characterization of NPs at the level of a single constituent is of utmost importance, in particular, if bottom-up techniques were used for the fabrication. These selfassembly techniques often lead to complexly shaped NPs or even to ensembles formed from many NPs composed of a large variety of different geometries [14]. In such cases the strongly geometry-dependent nature of the optical properties results in a featureless measured optical response when the measurements are conducted in solution. Then, all details from the individual structures are hidden in the ensemble average. However, most studies that aim for single particle spectroscopy only work reliable for rather large particles for which the scattering response remains notable. Particles with a size of at least few tens of nanometers can conveniently be analyzed by means of dark-field microscopy [15]. It can be also extended with spectroscopic equipment to analyze optical details [16] and not just accessing their location on a substrate.

In this work, We present synthesis of silver nano dimers by using silver clusters deposited onto a solid substrate using magnetic sputtering method. Furthermore, colloidal silver nanoparticles synthesized using citrate reduction method were linked together on the silver clusters with the help of linker like hexanediol.

2. Theory

2.1 Synthesis of Silver Nanoparticles

2.1.1 Chemical synthesis of AgNPs

The rapid growth of nanotechnology is directly related to the ability to design novel materials at the nanoscale level alongside recent innovations in analytical and imaging technologies for measuring and manipulating nanomaterials. The rapid development of commercial applications involves the use of a wide variety of manufactured NPs. Nanotechnologies hold great promise for reducing the production of wastes, reducing industrial contamination and improving the efficiency of energy production and use. However, the production, use and disposal of manufactured NPs will inevitably lead to discharges to air, soils and aquatic systems [17]. Silver nitrate is corrosive, causing burns in contact with the skin and eyes. Sodium borohydride is flammable and toxic [18].

DMF was a powerful reducing agent for silver ions. Colloidal silver particles in the nanometer size range were synthesized by reduction with DMF, using the silane coupling agent 3-aminopropyltrimethoxysilane as a stabilizer. The reaction rate was strongly influenced by temperature and by the Ag : 3-aminopropyltrimethoxysilane ratio, which also affects the mono dispersity and particle size of the colloids [19]. Polychrome silver nanoparticles were synthesized by microwave irradiation and chemical reduction of silver ions in different solvents with PVP. Silver nanoparticles with an average size of 32 nm were found. The solution was yellow and only one sharp symmetric absorption peak at 403 nm was observed in the UV-Vis spectrum [20].

Ethylene glycol was used as reducing agent for the synthesis of mono disperses samples of silver nanocubes. Controlling the size, shape, and structure of metal nanoparticles is technologically important because of the strong correlation between these parameters like optical, electrical, and catalytic properties. The major requirement seems to be the selection of a capping reagent that is able to chemically modify various faces of a metal with an appropriate selectivity [21]. When compared to the radiolytic reduction method, the citrate reduction method produced larger crystallites. Steady-state measurements as well as pulse-radiolysis studies show that citrate ions have a high affinity for silver nanoparticles. Citrate ions influence the particle growth at early stages by complexing with positively charged $Ag2+$ dimers. Fewer seeds formed in the citrate reduction method and slow cluster growth contributes to the formation of larger silver nanocrystals of varying shape and size [22].

Long aspect ratio silver nanowires may find applications in nanoscaled electrical circuits requiring long electrical connections. Wires with short aspect ratios find application relevant to the wireless telecommunication industries. A simple method for the preparation of silver nanowires by wet chemical approach has been reported. This method is based on the assembly of silver nanoparticles using a bi-functional alkyl thiol [23].

Langmuir-Blodgett is a powerful technique that can be used to assemble large-scale monolayers of hydrophobic silver nanoparticles on a water surface. The technique consists of spreading a thin film of a colloidal solution of Ag nanoparticles in an organic solvent on a water surface, which has a controlled convex curvature, and allowing the solvent to evaporate. As the solvent evaporates, a monolayer of silver nanoparticles nucleates at the raised centre of the water surface and grows smoothly outward. These monolayers could be transferred to a smooth substrate by bringing the substrate parallel to the water surface and lightly touching the substrate to the nanoparticle film [24].

Silver powder has been prepared through polyol route using glycerol starting from silver nitrate [25]. Production of silver nanowires using a polyol process, in which platinum nanoparticles were first produced by reducing PtCl2 with ethylene glycol at 160°C. These Pt nanoparticles could serve as seeds for the heterogeneous nucleation and growth of silver that was produced in the solution via the reduction of AgNO3 with ethylene glycol. Silver was to grow into uniform nanowires by adding poly(vinyl pyrrolidone) to the reaction mixture. These silver nanowires were bicrystalline, having uniform diameters that could be easily controlled in the range of 30-40 nm. Silver nanowires were synthesized using well dispersed suspensions in solvents such as water, alcohols, and acetone, without adding other surfactants [26].

Silver nanoparticles were prepared by the reduction of silver ions with formamide in the absence and presence of stabilizers such as poly(N-vinyl-2-pyrrolidone) and SiO2 nanoparticles. Attempt has been made to see the effect of addition of methanol, and a complexing agent on the stability of silver nanoparticles [27].

Silver wires were produced by a novel chemical reduction method of Ag-ions in an aqueous electrolyte solution which yields, both nanoparticles and nanowires [28]. Polychrome silver nanoparticles were prepared using the microwave technique using three solvents, nanopure water, ethylene glycol and glycerol. Effect of poly(vinylpyrolidone) on the stabilization of metallic particles was studied and compared with the reflux technique [29].

Ag nanoparticles were synthesized by silver salt (AgNO3) reduction with sodium citrate and transferred onto polymer modified silica (SiO2) and polyethylene terephthalate (PET). Size of the nanoparticles determined by comparing theoretical (calculations according Mie scattering theory) and experimental UV-VIS absorption spectrum results indicated dispersion of size around 100 nm [30].

One-pot reproducible route for the large scale preparation of polyacrylamidestabilized colloidal silver nanoparticles was exploited. The synthesis was done with only three reagents; silver nitrate, acrylamide and water. Neither the commonly used reductant nor initiator was used. The obtained silver colloids are stable and easy for purification with dialysis or centrifugation to remove nitrate ions and unreacted reagents. UV-vis spectrometry, previously used to monitor the growth of silver nanowires, was exploited to study the presence and removing of silver oxide layers covering the surface of silver nanoparticles. A possible mechanism for the formation of silver nanoparticles with bimodal size distribution was proposed [31].

Silver nanoparticles were prepared by a polyol process of silver nitrate in the presence of polyvinylpyrrolidone (PVP) with sodium carbonate [32]. Single-step route for the preparation of nanoparticle films over large areas and for conformal coatings on curved surfaces was studied. The method relies on in situ synthesis of nanoparticles followed by deposition on desired metallic and nonmetallic substrates under solvothermal conditions [33]. When silver nanoparticles solution has been doused with a ct-DNA solution, strong fluorescence signal was found. Based on this, a new spectrofluorimetric method was proposed for the determination of ct-DNA [34].

Synthesis of silver nanoparticles by an inert gas condensation method using flowing helium gas was studied. Helium was introduced into the process chamber after flowing it through a liquid nitrogen filled heat exchanger to maintain its cooling efficiency [35].

Spherical doping titania composite powders were synthesized by spray pyrolysis from an aqueous solution containing H2TiF6 and AgNO3. The particle size of powder can be controlled by adjusting the concentration of solution [36].

A new kind of stabilizer (an amine-terminated hyperbranched poly(amidoamine)) was used to produce colloid silver nanoparticles. This hyperbranched polymer was found to serve as a highly effective self-reducing agent. This method holds three advantages; (i) no extra reducing agent was needed, (ii) the process was conducted at room temperature under normal pressure and in aqueous solution, (iii) the obtained silver nanoparticles have several excellent properties, including long-term dispersion stability, small particle sizes, and a narrow size distribution controlled by the amount [37].

Au-Ag alloy nanoparticle was prepared on cellulose nanocrystal by the chemical reduction using NaBH4. Cellulose nanocrystal serves as a stabilizing template for the alloy nanoparticles [38]. Ag and Pt nanoparticles were successfully synthesized by hydrolysis of either Ag2Na or Pt-Na at room temperature. The oxidation of sodium in the Pt-Na pellets was much faster than that in the Ag-Na pellets since Pt is a catalyst for H2O formation reaction from hydrogen and oxygen at room temperature. The hydrolysis by-product (NaOH) was easily removed [39]. Synthesis of uniformly distributed Ag colloids by a simple and green route was described using polyethylene glycol as an environment-

friendly reducing agent and stabilizer, with H2O as green solvent [40].

The reduction and stabilization of Pt nanoparticles followed by self-assembly into nanowires in an aqueous -d-glucose solution was studied. Hydrothermal treatment initiated the reduction of Pt(IV) ions dispersed in a pH 8.0 -d-glucose solution. The Pt nanoparticles were stabilized with oxidized glucose molecules. The Pt nanoparticles continued growing into nanowires followed by transformation into cubic nanocrystals with a rough needle surface. TEM and FT-IR spectra revealed the role of carboxylate groups [41].

Novel one-step method of synthesizing monodisperse AuNPs using purified recombinant green fluorescent protein as the reducing agent was performed. For the synthesis of 5 nm AuNPs, the role of AgNO3 as well as the native structure of green fluorescent protein has been found to be critical. Using recombinant green fluorescent protein as the model system, it was adopted for the reductive synthesis of AuNPs [42].

The photoreduction of AgNO3 in the presence of sodium citrate was carried out by irradiation with different light sources (UV, white, blue, cyan, green, and orange) at room temperature. Silver nanoparticles obtained as a function of irradiation time (1–24 h) and light source was followed by UV-visible absorption spectroscopy. This light-modification process results in a colloid with distinctive optical properties that can be related to the size and shape of the particles [43].

Synthesis of uniform monodisperse crystalline Ag nanoparticles in aqueous systems has been developed by synthesized mono and dihydroxylated ionic liquids and cationic surfactants based on 1,3-disubstituted imidazolium cations and halogens anions [44]. Silver nanoparticles synthesized from the reduction of silver ions using ethanol was reported [45]. The role of pH in the green synthesis of silver nanoparticles was investigated. For the reduction synthesis, silver nitrate, glucose, sodium hydroxide and starch were used as precursor, reducing agent, accelerator and stabilizer [46].

Silver nanoparticles are considered to apply as silver paste for electrode because of their high conductivity. However, the dispersion of silver nanoparticles in electronically conductive adhesives restricts the use as conductive fillers. A simple method had enabled the synthesis of silver nanoparticles by reducing silver nitrate with ethanol in the presence of poly(N-vinylpyrrolidone). Reaction conditions such as silver nitrate concentration, poly(N-vinylpyrrolidone) concentration, reaction time and reaction temperature were studied [47].

Simple wet chemical route to synthesize nano-sized silver particles and their surface properties were studied. Silver nanoparticles of the size 40–80 nm were formed in the process of oxidation of glucose to gluconic acid by amine in the presence of silver nitrate, and the gluconic acid capped the nano silver particle. The presence of gluconic acid on the surface of nano silver particles was confirmed by XPS and FTIR studies. As the

nano silver particle was encapsulated by gluconic acid, there was no surface oxidation as confirmed by XPS studies [48]. Metal nanoparticles were synthesized continuously in supercritical methanol without using reducing agents at a pressure of 30 MPa and at various reaction temperatures ranging 150–400°C. Scanning electron microscopy showed that the particles size and morphology changed drastically as the reaction temperature increased. The average diameters of Ni, Cu and Ag particles synthesized at 400°C were 119±19 nm, 240±44 nm, and 148±32 nm, respectively. The supercritical methanol acted both as a reaction medium and a reducing agent [49].

Silver ions were reacted with O2 and CCl4 as electron transfer from the silver particles to the solutes stabilized with various polymers like polyethyleneimine, sodium polyphosphate, sodium polyacrylate, and poly(vinylpyrrolidone) [50]. Clay particles were expected to bind metal ions for effective protection from aggregation. Preparation of metallic particles in Laponite suspensions by addition of a reductant was examined. The particles obtained were characterized by using UV-vis spectrophotometry and transmission electron microscopy [51].

Synthesis of silver nanoparticles passivated with a surfactant, Nhexadecylethylenediamine was studied. A new procedure to synthesis silver nanoparticles using a N-hexadecylethylenediamine silver nitrate (Ag(hexden)2 NO3) complex was attempted. Nanocomposite, diamine-protected silver particles prepared from such a complex was expected to be completely free from the surface contamination caused by the conventional phase-transfer agent [52]. Direct method for preparing narrowly dispersed silver nanoparticles without using size-selection process by thermal reduction of silver trifluoroacetate in isoamyl ether in the presence of oleic acid [53] was studied. Citrate serves as reducing agent and as capping ligand for the silver nanoparticles, silver ions are reduced on the surface of the nanoparticles. The concentration of silver ions in solution controls the final size of the particles [54].

Synthesis of AgNPs by the solvothermal route, which was inexpensive and requires only simple precursors was reported. This method has been done with thiols of different chain length, such as octane and octadecane thiols, and the particle size was found to be nearly the same for both molecules [55]. In vapour-phase synthesis of nanoparticles, conditions were created where the vapour phase mixture is thermodynamically unstable relative to formation of the solid material to be prepared in nanoparticulate form. This includes usual situation of a supersaturated vapour [56]. Spontaneous formation of ordered gold and silver nanoparticle stripe patterns on dewetting a dilute film of polymer-coated nanoparticles floating on a water surface was studied. Well-aligned stripe patterns with tunable orientation, thickness and periodicity at the micrometre scale were obtained by transferring nanoparticles from a floating film onto a substrate in a dip-coating fashion.

Well-dispersed Ag nanoparticles are formed in situ on the surface of polystyrene (PS) core-

poly(acrylic acid) (PAA) polyelectrolyte brush particles by photoemulsion polymerization
of Ag-acrylate. Dynamic light scattering (DLS) measurement demonstrates the formation
of polyelectrolyte brushes onto the PS core surface [57].

Stable colloidal silver has been prepared by reduction of silver nitrate in the presence of
PVP. Kinetic feature of the PVP as a protect agent of stable silver nanoparticles in ethanol
was examined. The UV-visible spectroscopy provides information on the formation kinetics
as well as an indirect measure of the size and size distribution of the silver nanoparticles
[58].

Facile water-cyclohexane two-phase system to prepare monodisperse silver and gold
nanoparticles was developed. The aqueous formaldehyde was transferred to cyclohexane
phase via reaction with dodecylamine to form reductive intermediate in cyclohexane; then
the intermediate could reduce silver or gold ions in aqueous solution to form dodecylamine
protected silver and gold nanoparticles in cyclohexane solution [59]. Relatively few studies
have been reported on the mechanistic aspects regarding the formation and stabilization
of Ag nanoparticles. [60]. Electrochemical reduction of benzyl chloride was evaluated with
silver by cyclic voltammetry and interpreted in comparison with that of conventional silver
electrodes [61].

Photochemical synthesis of highly fluorescent functional silver nanoparticles was done.
These particles were very stable and can be reliably and reproducibly synthesized [62].
Citrate-stabilized silver nanoparticles prepared by both photoconversion and thermal
synthesis methods can be transferred to polar organics such as water, alcohols, acetone,
dimethylformamide and hexanes for stabilization purpose. Using sodium oleate as a phase
transfer agent, the silver nanoparticles prepared by both photoconversion and thermal
synthesis routes transferred to hexanes with up to 75% phase transfer efficiency [63].
Hollow single crystal silver nanospheres synthesized from silver oxide nanoparticles in the
water medium, being strongly kinetically controlled, bears resemblance to the nanoscale
Kirkendal effect [64]. A stepwise reduction method was developed for the preparation of
triangular silver nanoprisms in the absence of surfactant or special cappingagent. In this
approach, first a part of the precursor, silver nitrate, was reduced rapidly by NaBH4 to
produce small spherical silver nanoparticles at ice cold condition [65]. Silver nanowires were
synthesized though a solvothermal method. It was found that the addition of FeCl3 greatly
facilitates the formation of silver nanowires. Both the cation and anion are necessary for
the production of Ag nanowires. Silver nanowires with controllable sizes could be obtained
by adjusting the concentration of FeCl3 [66].

Silver nitrate (AgNO3) is the most widely used salt precursor accounting for almost 83%
of those reported in studies of general and specific synthesis methods. The dominant
27 use of AgNO3 is attributed to its low cost and chemical stability when compared
to other types of silver salts. Organic and inorganic solvents are used in the synthesis

of silver nanomaterials. Approximately 80% of synthesis processes use water as a solvent. NaBH4 (23%) and sodium citrate (10%) accounted for 33% of all the used reducing agents. Lesser percentages of other reducing agents were used in special synthesis applications. From an environmental perspective, although sodium citrate may not pose an immediate environmental threat as a reducing agent, NaBH4 may lead to contamination due to the hydrogen atoms in the BH4 anion.

Sodium citrate (27%) was the most commonly used stabilizing agent, followed by polyvinyl pyrrolidone (PVP) (18%), then amines (8%). Cetyltrimethylammonium bromide (CTAB), polyvinyl alcohol (PVA), sugars and amides accounted each for 5% of the stabilizing agents used in the reported research [67].

2.1.2 Green synthesis of AgNPs

Since prehistoric days human society use medicines, from gold, silver, mercury, sulphur, mica, arsenic, zinc, other minerals, gems, shells, horns treated with indigenous herbs as bhasmas and chendurams. A bhasma means a fine ash obtained through incineration. Chendurams are prepared by the process of sublimation and they are much more potent than bhasmas. Hippocrates explained the beneficial healing and anti-disease properties of silver. Ancestors used silver bottles for storing water, wine and milk to prevent spoiling. Siddha medicine is a form of South Indian medicine which is believed to have been developed by the Siddhars [68].

Owing to the need to develop environmentally benign procedures in the synthesis of metallic nanoparticles, plants, algae, fungi, bacteria, and viruses have been used for production of low-cost, energy-efficient and nontoxic metallic nanoparticles [69]. Green Engineering is the key weapon to tackle the needs [70].

DC arc-discharge between silver electrodes in pure water is a good alternative method, and is not only a relatively cheap process, but also environmentally friendly. The vapourized metal can be condensed more efficiently in the dielectric liquid than in the gas phase. Silver vapour condensed in water creates a stable Ag aqueous suspension. Well separated nano-sized Ag clusters in pure water seem to be thermodynamically stable for a long time [71].

Spontaneous reduction of silver facilitated by carboxylic acid groups in the presence of ambient light was tested. The peptides containing carboxylic acid functional groups facilitate reduction under ambient light and the reduction ability is dependent on the local concentration of silver ions associated with the conformation of peptide. It is suggested that tethering peptides to a biological scaffold enhances the reduction ability, and the surface density of the peptides on the scaffold determine the final nanostructure of silver [72].

Nanosilver was developed as a potent antibacterial, antifungal, anti-viral and antiinflamma-

tory agent. The enzymatic method of synthesis is suggesting that enzymes are responsible for the nanoparticle formation. The biomedical applications of silver nanoparticle can be effective by the use of biologically synthesized nanoparticles which minimize the factors such as toxicity, cost and are found to be exceptionally stable. The targeting of cancer cells using silver nanoparticles has proven to be effective [73].

Green synthetic methods include mixed-valence polyoxometallates, polysaccharide, Tollens, irradiation, and biological. The mixed-valence polyoxometallates method was carried out in water as an environmentally-friendly solvent. Eco-friendly bio-organisms in plant extracts contain proteins, which act as both reducing and capping agents forming stable and shape-controlled AgNPs. The synthetic procedures of polymer-Ag and TiO2– AgNPs are also given. Both AgNPs and AgNPs modified by surfactants or polymers showed high antimicrobial activity against Gram-positive and Gram-negative bacteria [74].

The process involves reduction of Tollens reagent under sonication at room temperature. By gradually adding Tollens reagent into the mixture of glucose solution and sodium hydroxide solution, the silver powder forms immediately without silver mirror formation at container wall [75].

Pt0 and Pd0 nanoparticles were prepared with various Mo(V)-Mo(VI) mixed valence polyoxometalates (POMs) in water at room temperature. These molecules contain synthetically built-in electron donor capabilities. The POMs were used as agent to prepare nanoparticles with soluble and stable in such media, and NPs obtained as new shapes, sizes, and properties [76]. Ag nanoparticles were formed by adding AgNO3 solution into the sucrose ester micellar solution containing sodium hydroxide at atmospheric condition after 24 h of ageing time. Trace amount of dimethyl formamide in the sucrose ester solution served as a reducing agent while NaOH acted as a catalyst. The Ag nanoparticles produced were highly stable in the sucrose ester micellar system as there was no precipitation after 6 months of storage [77].

Highly stable and hydrophilic ionic liquid-capped gold nanoparticles were synthesized by in situ reduction of HAuCl4 with NaBH4 in an aqueous medium. Two kinds of ionic liquids namely, 1-dodecyl-3-methylimidazolium chloride and a geminal-IL, 1,4-bis(methylimidazolium-1yl)dodecane bromide were used [78].

The AgNPs were stabilized by using oleic acid as a surfactant and used for the reduction of silver ammonium complex [Ag(NH3)2] + (aq) by glucose with UV irradiation treatment. A stable and nearly monodisperse aqueous AgNPs solution with average-sized particles 9-10 nm was obtained. The AgNPs exhibited high antibacterial activity against both Gram-negative Escherichia Coli and Gram-positive Staphylococcus aureus bacteria [79].

Platinum nanoparticles were prepared by the reduction of sodium borohydride in water. Electrocatalytic activity of the resulting nanosized Pt-1-(3-aminopropyl)-3-

methylimidazolium bromide particles toward reduction of oxygen and oxidation of methanol was explored. Preservation stability of Pt-IL was studied [80].

A catalytic system consisted of in situ synthesized palladium and rhodium nanoparticles stabilized by various ionic liquids [BMIm][PF6], [BMIm][OTf] and N(C6H13)4Br. Supercritical CO2 extraction was employed for the removal of the metal precursor ligands in the catalyst synthesis step as well as for the separation of the hydrogenation products. The potential of this concept is shown using the example of the palladium and rhodium catalyzed hydrogenation of acetophenone. The most efficient catalyst, Pd-[BMIm][PF6], exhibited good activity and excellent selectivity [81].

Bio reductive approaches to Ag, Au, Cd, Pt, Pd, SiO2 and TiO2 NPs using different biological system was studied [82]. Surfactin, a lipopeptide biosurfactant, was used to stabilize the formation of silver nanoparticles. Synthesis of silver nanoparticles using a borohydrate reduction was performed at three pH levels (pH 5, 7 and 9) and two different temperatures in the presence of surfactin [83]. The shapes of silver nanoparticles such as nanoprisms and nanosphere were evaluated by recording the TEM images and time-course UV-vis-NIR spectra [84]. Highly stable aqueous dispersed AgNPs was synthesized by gamma radiolysis with gum acacia as a protecting agent. The formation of nanosized silver was confirmed by its characteristic surface plasmon absorption peak at around 405 nm in UV–vis spectra [85]. Water was used as the environmentally benign solvent in the preparation of AuNPs in the presence of ultrasound. Sodium citrate dihydrate was used as as non-toxic reducing and stabilizer agent [86]. Solution-free synthesis of silver nanocrystals using sugar as the reducing cum stabilizing agent in ambient conditions was attempted. Silver foil was used as a precursor. Thermal decomposition of silver/sugar composite yielded silver nanocrystals [87].

2.2 Applications of Silver nanoparticles

AgNPs have been used extensively as anti-bacterial agents in the health industry, food storage, textile coatings and a number of environmental applications. It is important to note that despite of decades of use, the evidence of toxicity of silver is still not clear. Products made with AgNPs have been approved by a range of accredited bodies, including the US FDA, US EPA, SIAA of Japan, Korea's Testing and Research Institute for Chemical Industry and FITI Testing and Research Institute [88] [89] [90] [91].

As anti-bacterial agents, AgNPs were applied in a wide range of applications from disinfecting medical devices and home appliances to water treatment [92] [93] [94]. Moreover, this encouraged the textile industry to use AgNPs in different textile fabrics. In this direction, silver nanocomposite fibers were prepared containing silver nanoparticles incorporated inside the fabric. The cotton fibers containing AgNPs exhibited high antibacterial activity against Escherichia coli [95] [96].

Furthermore, the electrochemical properties of AgNPs incorporated them in nanoscale sensors that can offer faster response times and lower detection limits. For instance, [88] electrodeposited AgNPs onto alumina plates gold micro-patterned electrode that showed a high sensitivity to hydrogen peroxide [97].

Catalytic activities of nanoparticles differ from the chemical properties of the bulk materials. For instance, Köhler et al. showed that the bleaching of the organic dyes by application of potassium peroxodisulphate in aqueous solution at room temperature is enhanced strongly by the application of silver containing nanoparticles [98].

Furthermore, AgNPs was found to catalyze the chemiluminescence from luminol–hydrogen peroxide system with catalytic activity better than Au and Pt colloid [99].

The optical properties of a metallic nanoparticle depend mainly on its surface plasmon resonance, where the plasmon refers to the collective oscillation of the free electrons within the metallic nanoparticle. It is well known that the plasmon resonant peaks and line widths are sensitive to the size and shape of the nanoparticle, the metallic species and the surrounding medium. For instance, nanoclusters composed of 2–8 silver atoms could be the basis for a new type of optical data storage. Moreover, fluorescent emissions from the clusters could potentially also be used in biological labels and electroluminescent displays [100] [101].

2.3   Dimer Synthesis Mechanism

Dimer synthesis mechanism:

The exact mechanism by which NSDs form is uncertain though it may be due to the combination of G-Force, van der Waals, and electrostatic forces. Derjaguin, Landau, Verwey, and Overbeek (DLVO) theory and surface reconstruction may also help in describing the mechanism. Finally, fusion of two nanospheres may also be a result of the quantum effects of the Casimir force or cold welding.

2.3.1   G-Force, Weight by unit mass, inertial force

Researchers have used mechanical force to create and physically alter NPs, including nanowire and Au dimers. [102] Roca et al. hypothesized that the electrical double layer surrounding the Au NPs is polarized when under G-Force which attracts and binds the NPs together.[102] Au NPs in solution experience an electrostatic repulsion, but can experience electrostatic attractions when polarized under G-Force.[102] The group found that optical properties and geometric alignment of NPs are dependent on the magnitude of G-Force as well as the removal of the citrate buffer. [102] Binding occurs when the electrical double-layer is compressed, decreasing its repulsion, and van der Waals forces become the dominant force. Van der Waals forces are inherent to the NP and inversely proportional

to the sixth power of their separation. [103] Both the electrostatic repulsion and van der Waals forces are inversely proportional to the interparticle distance making G-Force an important parameter for their control. [103]

2.3.2   DLVO Theory

The electric double layer is the electric potential of the NP.[103] Widely used in colloidal science, DLVO theory relates the attractive van der Waals forces to the repulsive forces of electric double layer. Between two surfaces, a lowering of the electric double layer will result in a net attraction and the total interaction can be described as sum of van der Waal's attraction and electrostatic repulsion. As the two NPs are pushed close together, eventually their electric double layers will overlap, resulting in a repulsion which has a maximum based on the double layer thickness. At a certain distance very close, the repulsion reduces dramatically and van der Waals forces dominate, causing the two NPs to attract and combine. Slightly further away is the maximum repulsive force produced by the electrostatic double layer so as the double-layer is compressed, repulsion increases until the critical point where the forces between the particles become attractive and the particles instantly combine. [103] Stability of the NP is a function of the solution conductivity, Brownian motion, surface chemistry, and the balance of electrostatic repulsion with van der Waals forces. [102] The surrounding medium is particularly important as it influences the magnitude of van der Waals and electrostatic forces surrounding the NPs, allowing for aggregation or binding. [26] Further aggregation is prevented by electrostatic repulsions and the steric barrier of the capping agent. In particular, citrate Au NPs are electrostatically stable due to the citrate trianions adsorbed on their surface. [104]

2.3.3   Surface Reconstruction

Due to intermolecular forces, atoms within a crystal will align themselves in a period structure. However, there is a difference between the atoms within the bulk material and the atoms at the surface, since the surface only experiences the intermolecular forces from one direction, which results in a significant decrease in electron density at the surface.[105] This results in the surface atoms having an altered structure or position referred to as either a relaxation or a reconstruction. For most metals, the surface layer will contract slightly or shift in order to minimize potential energy. For 5d metals (Ir, Pt, Au) surface interactions or adsorption onto a surface can commonly cause a surface reconstruction in which one or more layers change their twodimensional structure as well as position in order to minimize stress or energy. [106] Surface reconstruction can either be conservative or non-conservative, where the number of atoms on a layer is more or less than before reconstruction began. The tendency of a metal surface to undergo reconstruction is based on numerous factors such as surface energy, surface stress, and interatomic force constants, many of which can be currently estimated experimentally using Scanning Tunneling Microscopy (STM) or computationally with density functional theory. [105][107][106] The

exact mechanism for surface reconstruction is still incomplete but Mansfield and Needs have devised the theory commonly cited by researchers.[107] Their theory states that surface stress is the driving force for the reconstruction, balanced by the amount of energy required to bring an extra atom onto the surface layer and the energy change brought onto the Au surfaces have a tendency to reconstruct and have been calculated to have bond-lengths approximately 10% shorter [107], and the energy of a surface atom is about 10 meV higher than that of the ideal bulk material.[105] Additionally, research has shown that a curved gold surface in contact with another gold surface will prefer to be flat rather than curved.[108] The curves will be "filled in" during rapid surface restructuring which may occur due to the reduction of the Laplace pressure which reduces the free energy of a molecule at a curved surface. [109] Further study into surface reconstruction is useful not only for our understanding of the physical phenomenon and self-assembly, but also for applications in advanced circuits and optoelectronic devices.

2.3.4   Casimir Force

The Casimir effect or Casimir-Polder force is the physical attractive force of two electrically neutral objects with nanometer separations that is a result of fluctuations in zero point energy in an electromagnetic field and can be described by quantum field theory.[110] When two conducting parallel plates are very close (for example, 10 nm), vacuum electromagnetic energy density in between the plates will be less than outside, resulting in an attractive pressure. [111] The force is nonlinear and increases rapidly at distances less than 500 nm. [112] This results in a net attraction because there are less electromagnetic modes between the plates. Making two plates extremely parallel (105 rad for 1 cm plates) is very difficult in practice, so it has been common to measure the Casimir effect between a flat plate and sphere, avoiding the issue of parallelism to experimentally validate the theory. [[112] Recently, an international group overcame the issue of parallelism through electron-beam lithography and achieved separations of 70 µm. [113] The Casimir and van der Waals forces are related, but the Casimir force can be attractive or repelling depending on the geometry as theorized by Liftshitz. [114] For example, two plates will attract, while two hemispheres of a split sphere will repel; additionally, two bodies in liquid medium can be either repulsive or attractive. [112] [115] Some groups want to harness this repulsive force for use in MEMS or Nanoelectromechanical systems (NEMS), circuits, sensors, or for extremely low-friction devices.[113] [116] The Casimir effect is one of the many interesting quantum phenomenon that we see at the nanoscale.

2.3.5   Cold Welding

Some groups have reported the phenomenon of "cold-welding", "capillary wetting", or "sintering" of NPs which results in the merging of two metal NPs under low loads and without the need for heating. [117] [118] [119] The process occurs when NPs are pressed together or come in contact with their capping agent removed. The combination of the

NPs occurs abruptly when a critical pressure or interparticle separation is reached. [109] [108] When the atoms of two similar metal NPs are in contact, there is no way for the atoms to "know" which NP they are a part of. [120] Alcantar et al. found the "jump-in" point to be 10 nm, concluding that a mechanism or force other than just van der Waals must also be taking place in order to be attractive at that distance.[109] Similarly, Knarr et al. found the "jump-in" point to be at about 25 angstroms.[108] Both research teams found that the two Au surfaces had indeed become one and, afterwards, proceeded to pull the two surfaces apart. Again, both groups reported the same interesting finding: the Au surfaces didn't break at the newly formed interface but, instead, the Au broke from its mica substrate and remained bound to the other Au surface. The materials do not necessarily have to be the same composition as Au NPs have been stably "welded" to Ag NPs without detectable alloying. [117] Interestingly, it was also found that when different metals such as Ag and Au were cold-welded together, the Ag NPs seemed to behave as a soft material that "wets" a Au NP. Additionally, the detrimental effect of "dirt" or organic layers is significantly lower than expected. [109] [119] As our know-how continues along with our ability to fabricate and manipulate structures at the nanoscale, improvements to health, industry, and everyday life will become obvious.

2.4   Nanoscale modifications of surfaces

The modification of surfaces at the nanoscale is a technique of relevance in today's industry in multiple areas, particularly in electronics, where the production of surfaces with insulating, superconducting, ferroelectric or piezoelectric capabilities is of great interest [121]. Recently the interest of surface modification has been shifting to the medical and biological realm, as a way of improving implants or studying the behaviour of living microorganisms. There are many techniques for producing these modifications such as those depending in light beam sources (like pulsed laser deposition (PLD)) or techniques depending in other physical and chemical phenomena (plasma spraying, physical/chemical vapour deposition (CVD) and solvent evaporation)[122]. In the following figure it can be observed a sample of the different ways in which a surface can be modified.
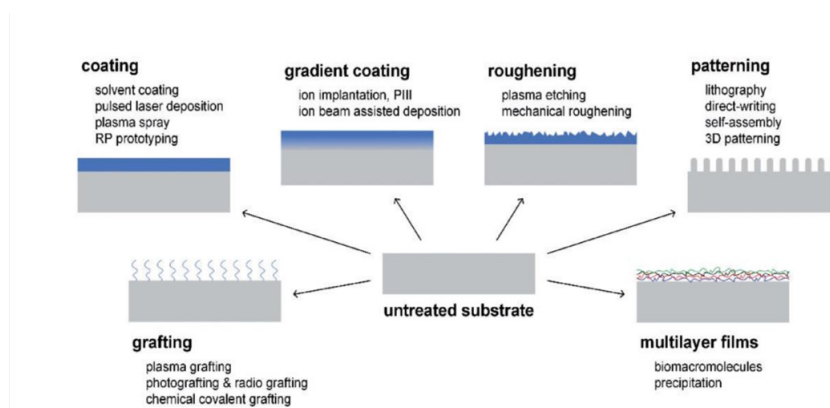
Figure 2.1: Different ways of modifying surfaces [122]

As it was said previously, the development of surfaces with particularities at several levels is beginning to be seen as a necessary step in the preparations of cell cultures. The characteristics of the microenvironment in which this cells are cultured, composing materials and topography, are of great importance in the final outcome of the aforementioned culture, although little is known about the exact effects they have. The variation of these parameters will obtain different responses from different cell lines; it is particularly true for stem cells since a variation in their overall environment will lead to drastic changes in its physiognomy, i.e. differentiation. This reality, by itself, is already an interesting topic of study that has inspired a plethora of experiments, but in this project the focus will be solely dedicated to the microenvironment characteristics, composing material, namely titanium, and the topography on a nano-scale level. Many efforts are being directed to obtaining a deeper understanding of the topography effect in cell development, particularly in stem cells; a field in which there is much to gain and the stakes are high, but the state of the art is not that advanced and more efforts will be necessary to produce reliable results. In this particular case, with the aim of pushing PDL cells into differentiation to osteoblasts, a nano-scale modification of a culturing surface made of titanium was produced. Its details will be exposed later on at the corresponding sections, for now, a more general approach to the theory and past experiments involving these modifications follows.

2.5   Modification of surfaces by cluster beam technique

A cluster is an aggregate of atoms or molecules, their number can range from a few up to many thousands. Thus, an atomic cluster can have a diameter on nanometre scale and often is called a nanoparticle. The clusters, due to their dimensions, have properties that are between the individual atoms (discrete levels of energy) and the bulk material (bands of states). This particular properties spark interest in many different areas such as basic material research in physics and more specific and applied research in electronics and

biology/medicine. Figure 2.2 shows studies done about the topic of energy levels in silver clusters, and the differences in behaviour that occur when the size of the metal under study is varied. In bulk metal the metal atoms share all their valence electrons forming a uniform and homogeneously distributed field, therefore they are good conductors, but the energy levels become a continuum with no gaps, the electrons have no barriers when populating the conduction band. As the size of the metal starts to get similar to that of the electron path the movement of electrons becomes restricted to that size (nanoparticle), primarily in the surface. This leads to plasmon resonance effects in this nanoparticles. When reaching lower sizes, clusters, the diminishment of the number of atoms causes the band to be divided in energy levels that no longer conduct energy well since they are further apart. The plasmon resonance effects no longer take place.
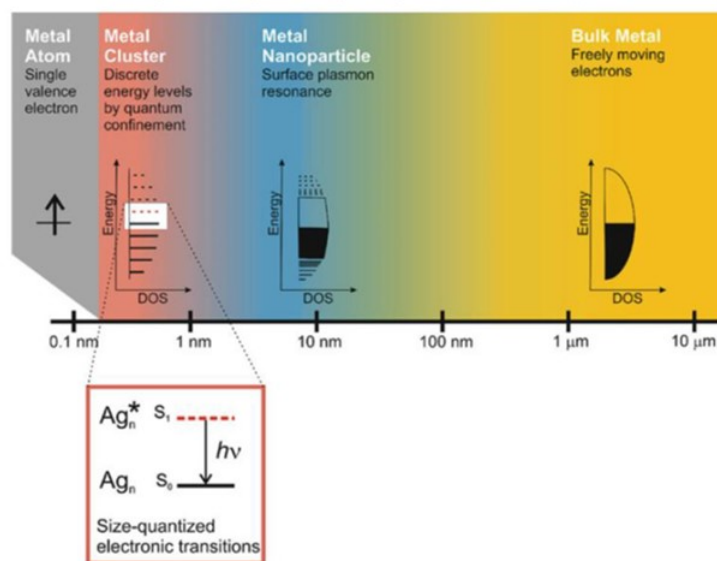
Figure 2.2: Diagram of the behaviour of materials depending on their size. Metal clusters find themselves halfway between individual atoms and bulk metals

To form the aforementioned cluster beams there are multiple techniques for surface erosion, that allows to sputter material from a bulk state and create conditions for aggregation of sputtered atoms into clusters, being the most popular ones arc discharge, laser vaporization and magnetron sputtering.

The magnetron sputtering was done within a machine known as the MaSCA. In this machine, central piece of this projects development, the sputtering source would provide the nanoclusters. More details are presented in the method part. More exactly, in a bottom-up approach, it produces atomic or molecular clusters in a gas phase that is then collimated into a beam, hence the name of cluster beam technique. Once in the beam these clusters will be deposited in surfaces of interest Cluster beam technologies provide with many advantages such as the control over the size and kinetic energy of clusters when being deposited on the surface, being the differences in the kinetic energy upon landing of great

importance, as they define the nature of the resulting product. It is by alterations on the kinetic energies of the produced clusters that the distinction between soft-landing (Figure 2.3) and higher impact energies (Figure 2.3) is made. Soft-landing is considered to be a situation in which the kinetic energy of each atom of the formed cluster is below the cohesive energy of the cluster components (around 0.1 eV, although the process depends on many other variables). It is of importance to mention that both size and material composition of the clusters will be of relevance in the outcome of the deposition. The fragmentation and the implantation rate increase as does the kinetic energy but fragmentation is diminished as the cluster size increases. Due to this, soft-landing depositions do not lead to cluster fragmentation, erosion of the surface or formation of craters and hillocks on it. Instead the clusters retain the original shapes (spherical) but with small variations, a little bit shorter, due to the physisorption (negligible perturbance on the electronic structure of an atom/molecule that has been absorbed); it is particularly true if the energy of each individual atom is close to the cohesive force of the constituents of the nanocluster and if there are interactions of the clusters and the atoms of the surfaces by means of Van Der Waals [123].
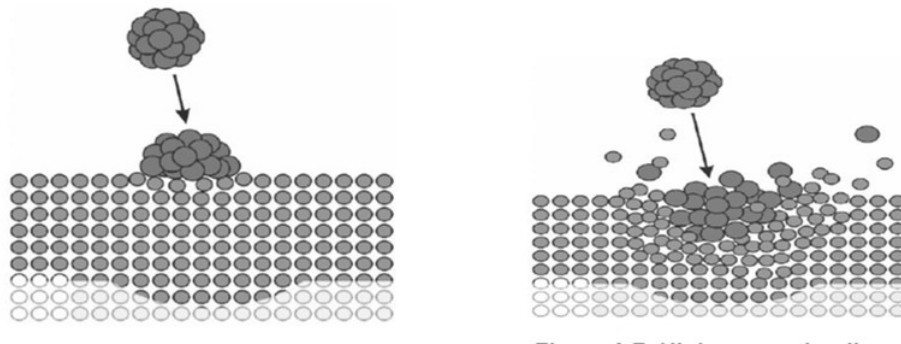
Figure 2.3: Soft landing(left) and High energy landing (right)

Since the unique properties of the clusters are of interest in many areas it is desirable to preserve to the best of possibilities; thus the soft-landing was chosen. At these low levels of energy other factors to which attention must be paid arise, one of them being the surface diffusion of clusters over the surface. This cluster mobility is more usually related to weakly interacting materials; if the lattice mismatch between cluster and surface is high enough to allow their vibrational coupling to overcome the small energy barrier of surface potential it can observed Brownian movement in the clusters over the surface. Particles under these circumstances can interact and either coalesce (merging of two or more small clusters into a larger particle of different shape) or agglomerate (in metal clusters of larger size, formation of ramified islands of material). If these circumstances were not to happen, clusters would remain motionless and isolated, forming submonolayer coverages and eventually a thin film [124]. Another problematic situation is the fact that 'roaming' particles tend to accumulate on the defects of the surface. Rate of diffusion of different metal clusters will also depend

on temperature and the material of which they are made of, but the lateral diffusion will be lower because of the interatomic interactions between the nanoclusters and substrate, particularly if they are made of the same material. It has been shown in previous studies that, for example, silver clusters deposited in a silicon layer at room temperature have low mobility in said layer, nevertheless, when deposited in highly ordered pyrolytic graphite (HOPG) the mobility would increase, as seen in figure 2.4 [123].
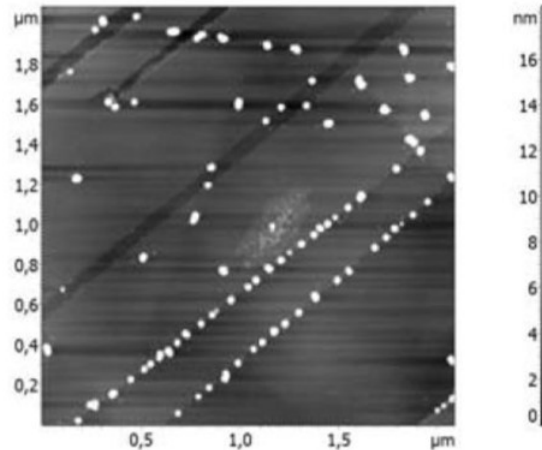

Figure 2.4: AFM image of silver clusters deposited on HOPG. The silver clusters line perfectly in a defect of the surface [123]

As would be predictable, depending on the surface material and the treatment that might have altered the materials characteristics, the landing of the nanoclusters will vary, leading to a lesser shape corrugation, a variation in highness in the deposited clusters or even change in the optical properties of the material. This dependence is related to substrate properties such as surface energy, corrugation, polarizability, temperature and hardness. On metallic surfaces it is common for small nanoclusters (100 atoms or less) to suffer changes in their distribution due to the interaction energies of the cluster with said surface whereas in other surfaces (e.g. MgO) the structure remains almost as it was in the gas phase. It is on these metallic surfaces that there will almost always occur a partial implantation of the nanoclusters as well as an atomic site exchange. From these findings it can be extracted that for small clusters in metallic surfaces soft landing does not provide a means of preserving the original structure of the nanoclusters for there will always be an atomic rearrangement, even at very low kinetic energies. As the size of the nanocluster grows to be considered a big cluster (several hundreds to thousands) the relevance of the interaction energies between nanocluster and surface diminishes, gaining the kinetic energy importance in the outcome of the soft-landing. In these cases, if the attraction of the surface is low there might not even have a deposition; if the attraction forces are higher, a metal surface, and the nanocluster is of metallic nature, the most probable conformation will be a monoatomic layer; it is only at low temperatures that 3D structures will thrive

[125].

Although in the past it has been shown that antimony and gold clusters diffuse, and agglomerate forming ramified islands, when deposited in HOPG due to the weak bonds they form [126], thin films formed of gold clusters strongly bonded to a gold substrate at room temperature and under high vacuum. This is due to the strong interactions between the clusters and the substrate; these clusters in direct contact to the substrate develop epitaxy to it. This epitaxy can extend to the clusters deposited above these first clusters but it will be thickness dependent, the thicker the less the epitaxial growth will be found in the second layer of clusters. These second clusters will have their structure affected by the tendency to match the lattice of the first cluster layer and the internal energies that keep its original shape. The final morphology will also depend on the size of the clusters and its incident energy, the bigger they are the harder it will be for the to "get epitaxial"; the higher the energy in impact the easier it will be for the rearrangement and coalescence of clusters, event that will lead to a more compact thin film [124]. Similar outcomes to those of the antimony and gold in HOPG can be found with the deposition of silver (isotope 160) on the same material and antimony (isotope 36) in amorphous carbon. Gold nanoclusters (isotope 250) on graphite also diffuse but through a careful study of the formed ramified islands it is postulated that agglomeration of the clusters is only partial in comparison with the previous examples and that even the smallest islands diffuse over the substrate [127]. In the case of gold (isotope 250) on NaCl it was reported a low level of mobility, due to the epitaxy preventing the clusters to move on the surface [128]. Regardless of what is known, soft-landing still pose many questions unanswered about its physical aspect. As the kinetic energy of the system (nanocluster + surface) increases so does the capabilities of the system of deriving to more energetically favourable structures. This affects the epitaxy degree, all the more if the nanocluster material coincides with the surface material, which would be the situation of the project, as the titanium nanoclusters will be deposited over a titanium substrate, if it were not for the fact that due to the chemical characteristics of titanium (as explained in the previous section) it almost instantly develops a surface of different titanium oxides, mostly titanium dioxide, when exposed to the ambient. Coming back to the nature of epitaxial growth, in past examples with copper, a large degree of epitaxy has been observed. If the components of both nanoclusters and surfaces were to be metallic but not of the same material, "the different melting points and atomic radii of the metals would affect the diffusivity of the individual atoms and result in pronounced wetting and epitaxy" [125]. Apart from the effect that the initial impact has on the epitaxy degree of the nanocluster, over time the behaviour of atoms has an effect on it as well. The way atoms move between the parts of the nanocluster with a degree of epitaxy and the disordered ones are of great effect on nanoclusters deposited in surfaces made of the same material [125].

3. Materials and Methods

3.1 Chemicals and instruments

Material	Manufacturer	Description
Acetone	Sigma Aldrich	$> 99.5\%$
Ethanol	Sigma Aldrich	$> 99.9\%$
Chloroform	Sigma Aldrich	99.9%
Silver Nitrate	Sigma Aldrich	
Trisodium citrate dihydrate	Sigma Aldrich	
1-Hexanethiol	Sigma Aldrich	
Poly(methyl methacrylate) PMMA	Sigma Aldrich	

Table 3.1: Materials used in this project

Equipment	Manufacturer	Description
Mangetron Sputtering Cluster Apparatus		
Centrifuge	Eppendorf	5804R
UV Vis NIR spectrophotometer	Perkin elmer	UV-1800
NanoSight LM10	Malvern	Sample chamber, microscope and camera
NanoSight NTA 3.2	Malvern	Software
nanolaboratory NTEGRA Aura Atomic Force Microscope	NT-MDT	

Table 3.2: Equipments and software employed in this project

3.2 Synthesis of Colloidal Silver Nanoparticles

Silver nitrate and trisodium citrate were used as starting materials for the preparation of silver nanoparticles. The silver colloid was prepared by using chemical reduction method.

All solutions of reacting materials were prepared in distilled water. In typical experiment 50 ml of 0.001 M AgNO3 was heated to boil. To this solution 5 mL of 1 % trisodium citrate was added drop by drop. During the process, solutions were mixed vigorously and heated until change of color was evident (pale yellow). Then it was removed from the heating device and stirred until cooled to room temperature.

The colloidal solution of silver nanoparticles were characterize by using UV-Visible spectroscopy, Atomic force Microscopy (AFM) and Nano particle tracking Analysis (NTA).

3.3   Synthesis of Dimers

The Cu and Ag clusters were prepared using MASCA instrument on a PMMA coated quarts surfaces. The CU cluster surfaces were further treated with ozone for 30 min to prevent further oxidation and annealed $120°$ for 1 min. While, the Ag cluster surfaces were not treated with Ozone. The Ag Cluster surfaces were also annealed at $120°$ for 1 min.

Now, the annealed surfaces were coated with 1-Hexanediol, which works as a linker for dimers, in a decicator under a constant argon flow for 1 hour. The surfaces were carefully removed from decicator and The colloidal AgNP solution was loaded on the surfaces and kept undisturbed for 10 min.

The surfaces were further airdried using nitrogen flow and then characterized using AFM and UV visible sprectroscopy.

4. Instrumentation

UV visible spectroscopy was performed at a path length of 1 cm using Shimadzu UV spectroohotometer (UV-1800). It measures the intensity of light passing through a sample (I), and compares it to the intensity of light before it passes through the sample (I_0) . The ratio I\I_o is called the transmittance, and is usually expressed as a percentage (%T). The absorbance, A, is based on the transmittance:

$$A = -log(\%T\backslash100\%)$$

Molecules containing π-electrons or non-bonding electrons (n-electrons) can absorb the energy in the form of ultraviolet or visible light to excite these electrons to higher anti-bonding molecular orbitals. The more easily excited the electron, the longer the wavelength of light they can absorb. There are four possible types of transitions (π- π^*, n-π^*, σ-σ^*, and n-σ^*).

Nanoparticle tracking analysis was performed using Nanosight LM10 (Malvern) instrument and Nanosight NTA 2.2 software to record multiple scans of the samples and data was processed to plot the size distribution curves.

Atomic Force Microscopy was performed using nanolaboratory NTEGRA Aura (from NT-MDT) instrument was used. Height analysis and height distribution was calculated using WSXM software.

5. Results and discussion

5.1 UV visible spectroscopic analysis

Optical properties were studies using UV visible NIR spectroscopic analysis. The prepared surfaces were placed in a 1 X 1 cm sample holder and the spectra was recorded.

The Ag cluster surfaces were analyzed after cluster deposition, after annealing and after AgNP colloidal particles were loaded onto them. A comparative spectra can be observed below. Here 120 and 180 are the numbers used for identification of 2 different samples (the quarts substrate was baked at 120° and 120° temperatures after PMMA coating).
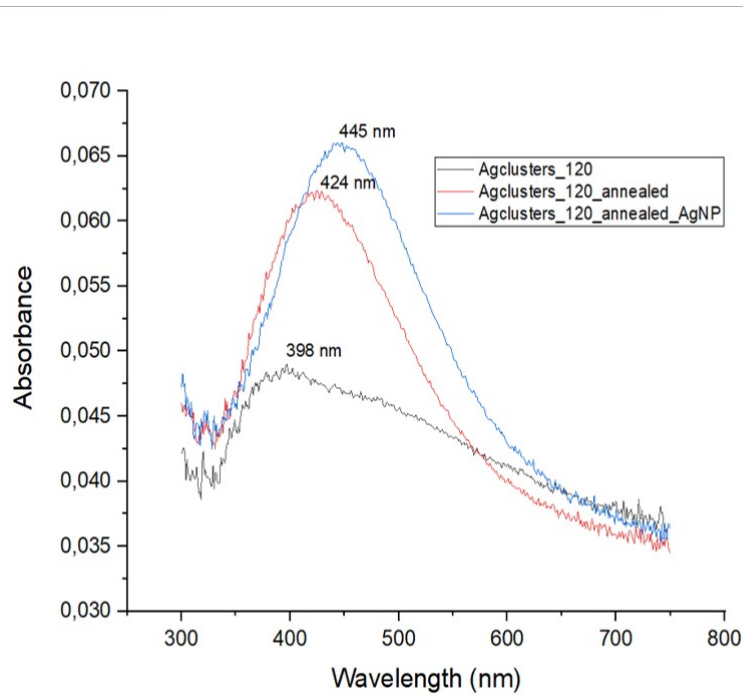
Figure 5.1: UV visible spectroscopic analysis of Ag clusters 120 at different stages

As we can observe in the above graph,a broad peak at 398nm wavelength is observed with low absorbance intensity (black curve) for Agcluster120 sample before annealing. The broad peak could be because of presence of poly-disperse particles. While after annealing (red curve), we observe a red shift in the spectra with increased absorbance intensity. One possibility could be due to annealing, the particles become well structured and also it was observed in AFM images that they slightly get embedded in the PMMA surface leading to increasing their stability.

Whereas,after loading colloidal AgNP particles (blue curve), we observe slightly more red shift as well as increased absorbance intensity. Here, we can hypothesize that due to the surface plasmon properties of the colloidal AgNP particles also contribute in the spectra and which leads to increased absorbance intensity and due to the bigger size of the colloidal particles we observe a red shift.
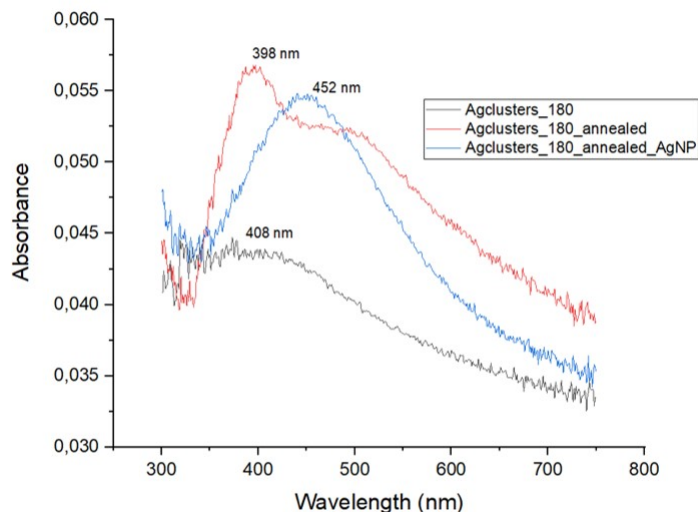
Figure 5.2: UV visible spectroscopic analysis of Ag clusters 180 at different stages

While, in the Agclusters180 sample, we can observe a broad and damp peak at 408 nm (black curve), while we can see a blue shift after annealing (red curve) leading to a peak at 398 nm with increased intensity of absorbance. We can give the same explanation like the previous sample for the shift and increased intensity. But interestingly, we can observe a second peak around 500 nm. This could be because of the SPR effect of two particles contributing to the spectra.

After loading the AgNP colloidal particles, The second peak is seen to be disappeared and we observe a high intensity peak at 452 nm. The possible reason for this behaviour could be etching between two particles and formation of the dimers. [129]

The absorbance decreased towards higher wavelength and reaches close to zero near the visible wavelength region. The absorbance is concentration dependent and the Full width half maximum value increases with increasing concentration.

5.2   Nanoparticle tracking analysis

The size distribution of AgNP synthesized using citrate reduction method was analyzed to study the possible application of the synthesized nanoparticles. The sample stored in a cool

condition to avoid agglumeration of the particles and brought back to room temperature before analyzed in a NanoSight sample chamber.
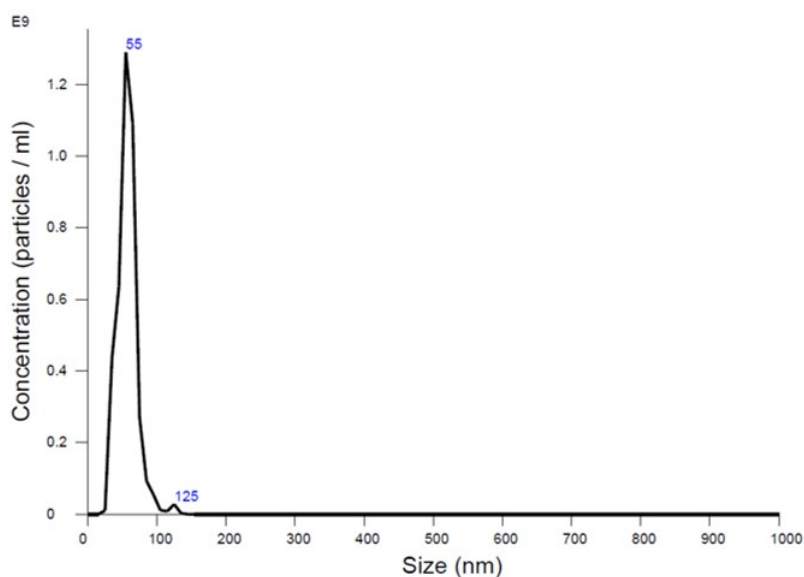
Figure 5.3: Size distribution of colloidal AgNPs synthesized with citrate reduction method. Multiple scans were performed

The size distribution plot can be seen in figure above. As we can see, a very sharp and narrow pic with high intensity was recorded around 55nm. Most of the particles in the sample were recorded to be having their hydrodynamic diameter between 10 to 90 nm size. The mean size was found to be 57 nm. While some smaller peak was recorded at 125nm. These smaller peak could be due to coagulated particles or may be because of some impurity.

5.3 AFM analysis of Colloidal AgNPs
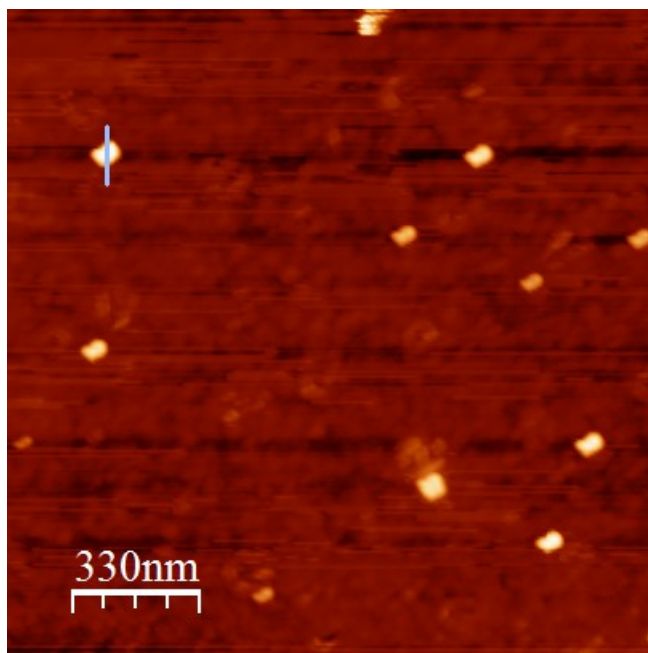
Figure 5.4: AFM image of colloidal AgNPs synthesized with citrate reduction method. Multiple scans were performed

The topographic image above shows a nice distribution of colloidal AgNP synthesized using citrate reduction method. As it can be seen in the below image, during the profile analysis one particle was measured to be at 25 nm height from the Gold surface.
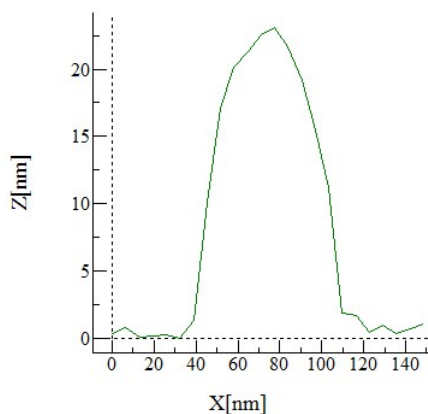

Figure 5.5: Height analysis of colloidal AgNPs synthesized with citrate reduction method. Multiple scans were performed
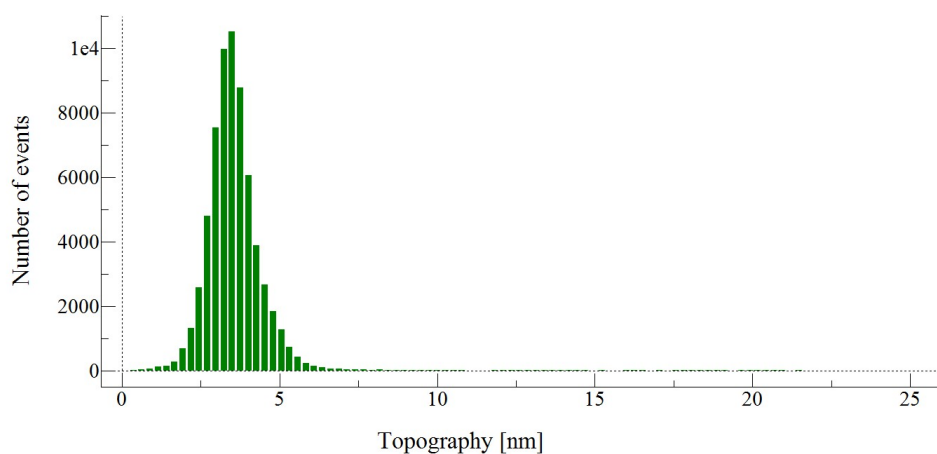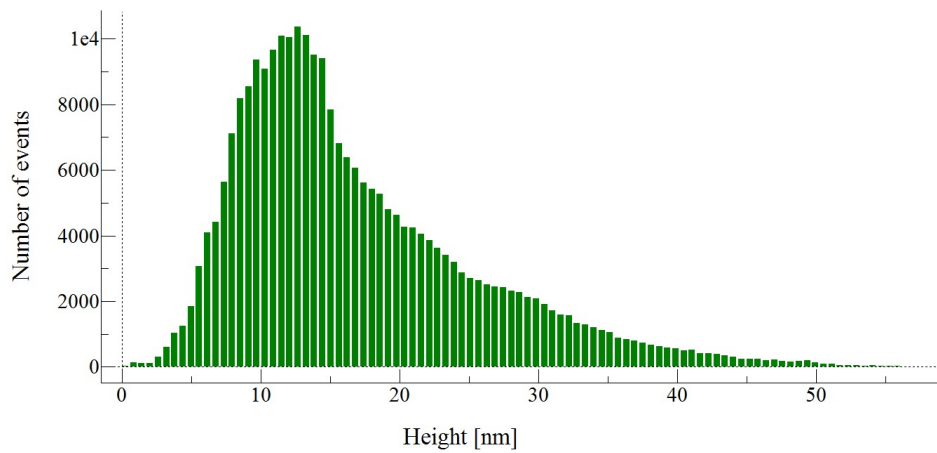
Figure 5.6: Height distribution of colloidal AgNPs

From the nanocluster height study it can be seen that there is a Gaussian distribution in the height of the clusters in a range from 3 nm until a little over 22 nm. In the range from 3 to 9 nm height most of the deposited nanoclusters were found.
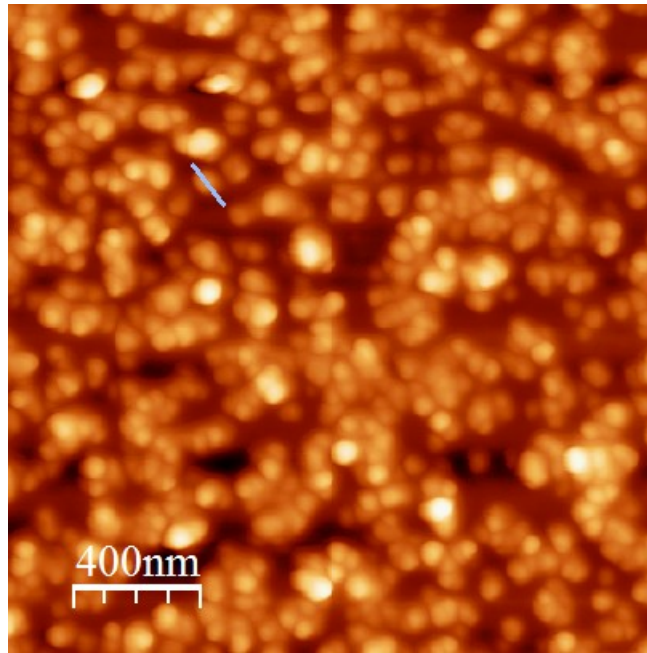
5.4   AFM analysis of Cu clusters+AgNP dimers
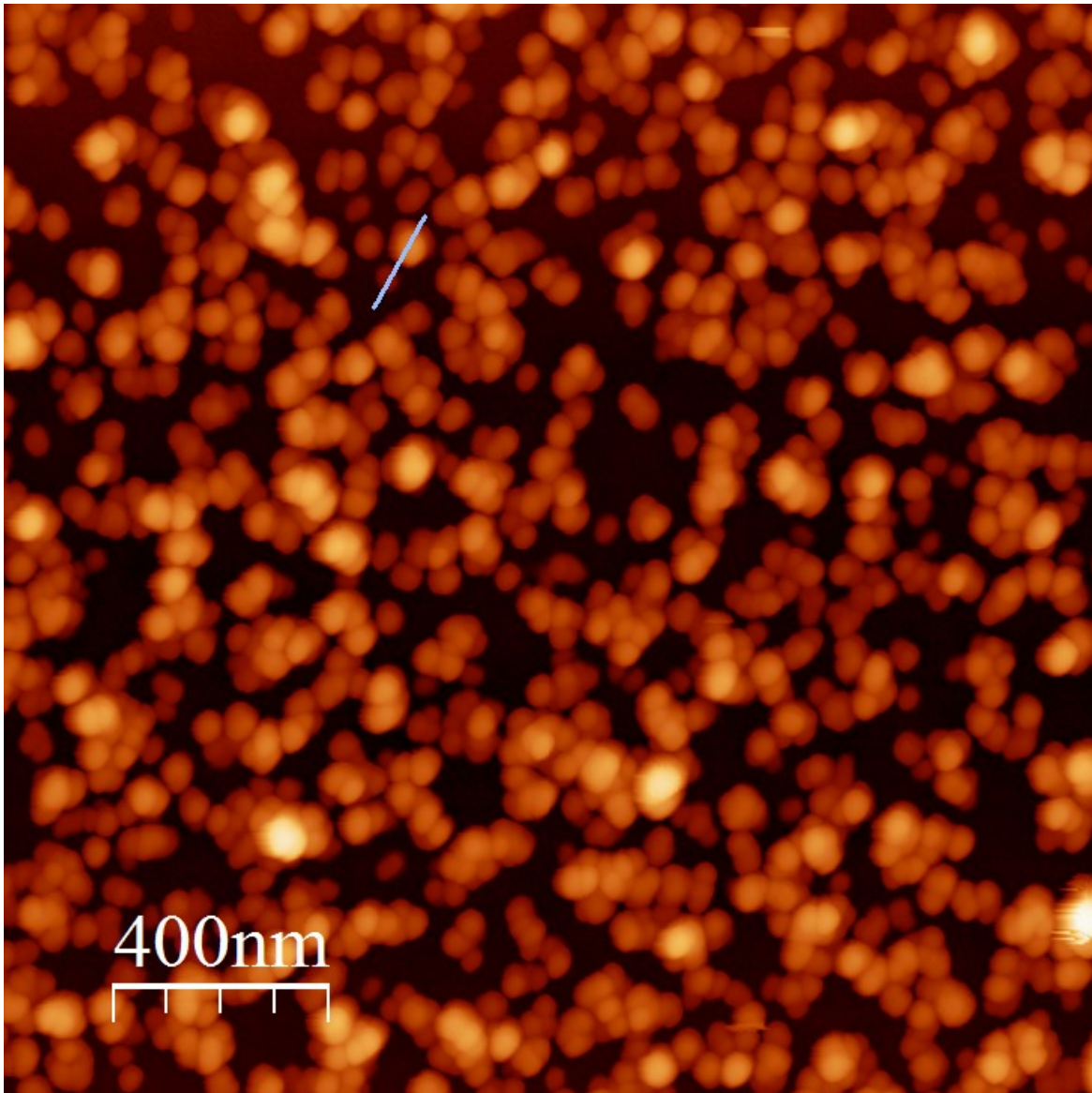
Figure 5.7: AFM image of Cu clusters+120

The topographic image above shows a nice distribution of Cu clusters+120.   The distribution of the clusters is very dense and they seem to be deposited at different height from the PMMA surface. As it can be seen in the below image, during the profile analysis one particle was measured to be at 50 nm height from the PMMA surface and one was measured to be at 10 nm height.
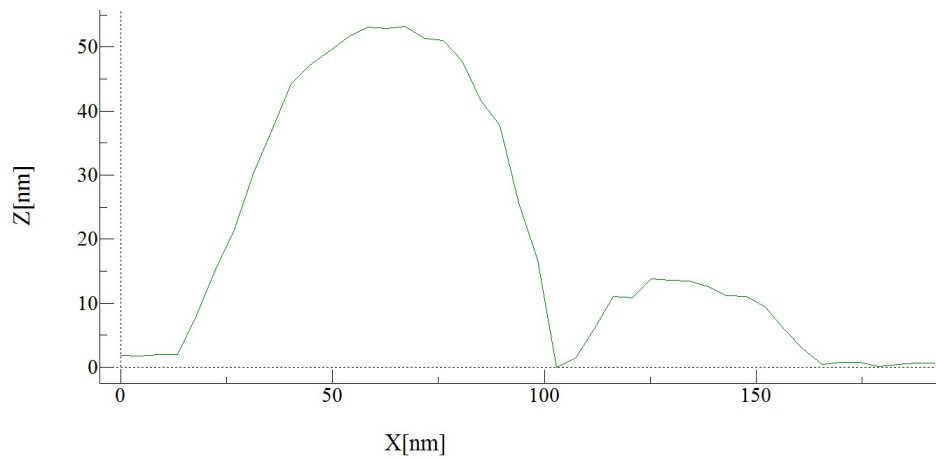
Figure 5.8: Height analysis of Cu clusters+120
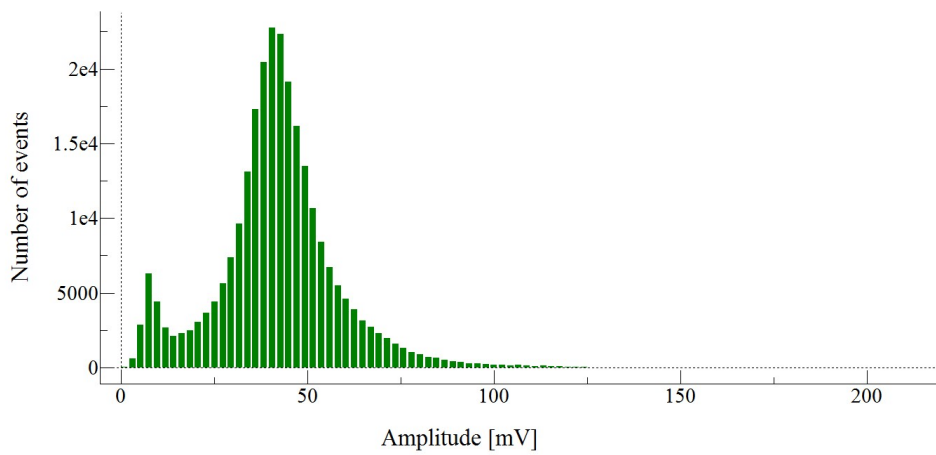
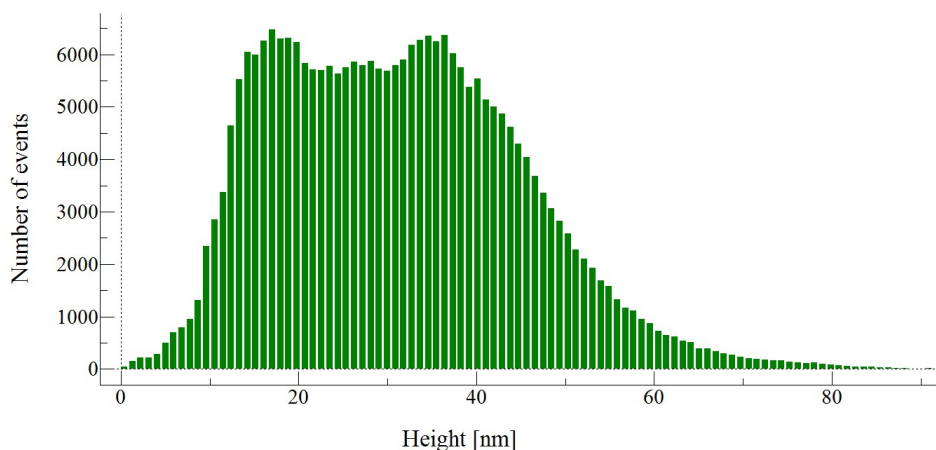**Figure 5.9:** Height distribution of Cu clusters+120

From the nanocluster height study it can be seen that there is a Gaussian distribution in the height of the clusters in a range from 5 nm until a little over 100 nm. In the range from 25 to 60 nm height most of the deposited nanoclusters were found.
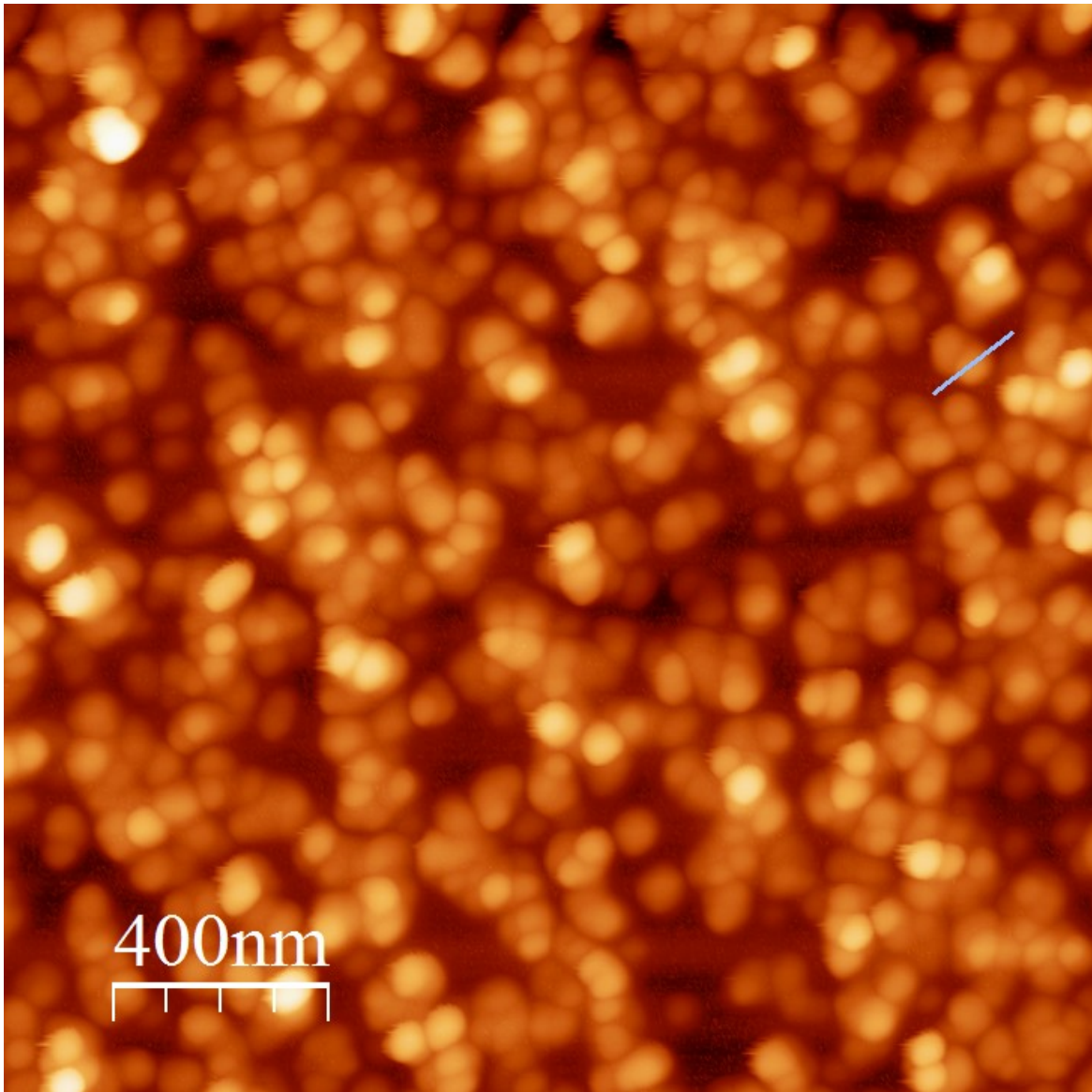
Figure 5.10: AFM image of Cu clusters+120+ozone

The topographic image above shows a nice distribution of Cu clusters+120+ozoned. The distribution of the clusters is very dense and they seem to be deposited at different height from the PMMA surface. Furthermore, the sample is observed after ozone treatment fro 30 min. Because of the ozone treatment, the particles appear to have formed a layer surrounding them to prevent them from further oxidation. As it can be seen in the below image, during the profile analysis one particle was measured to be at 33 nm height from the PMMA surface.
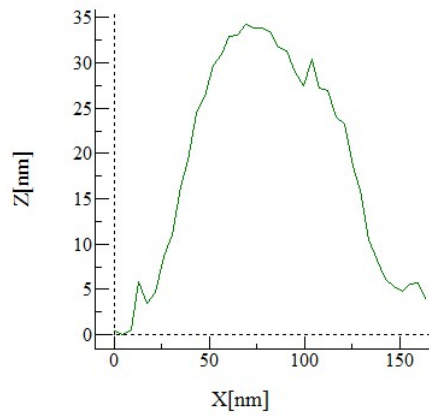
Figure 5.11: Height analysis of Cu clusters+120+ozone

Figure 5.12: Height distribution of Cu clusters+120+ozone

From the nanocluster height study it can be seen that there is a Gaussian distribution in the height of the clusters in a range from 5 nm until a little over 45 nm. In the range from 10 to 15 nm height most of the deposited nanoclusters were found.
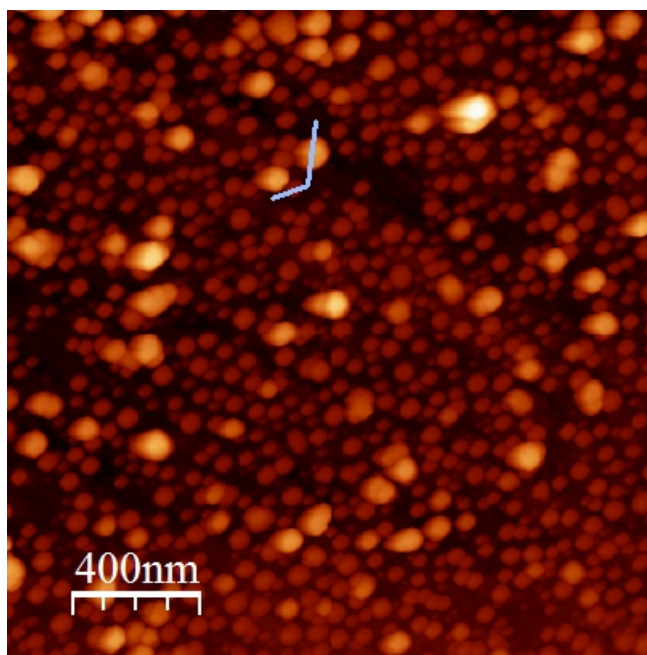
Figure 5.13: AFM image of Cu clusters+120+ozone+annealed

The topographic image above shows a nice distribution of Cu clusters+120+ozoned+annealed. The distribution of the clusters is very dense and they seem to be deposited at different height from the PMMA surface. The sample is after annealing process, so ideally some of the particles should get embedded into the PMMA and thus we expect the height analysis to show less height than the previous sample. But that is not the case. As it can be seen in the below image, during the profile analysis one particle was measured to be 35 nm. But the overall height distribution range was observed to be decreased.
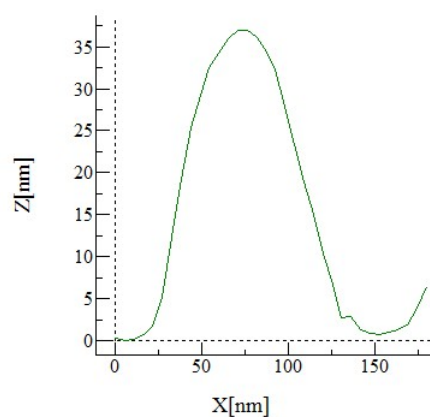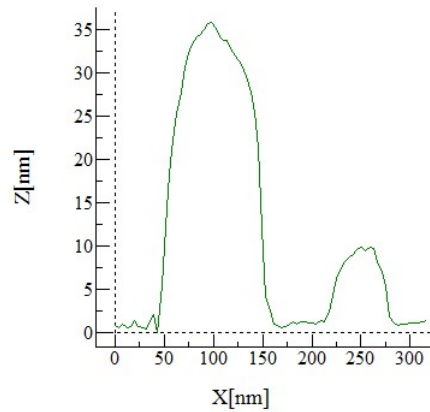

Figure 5.14: Height analysis of Cu clusters+120+ozone+annealed

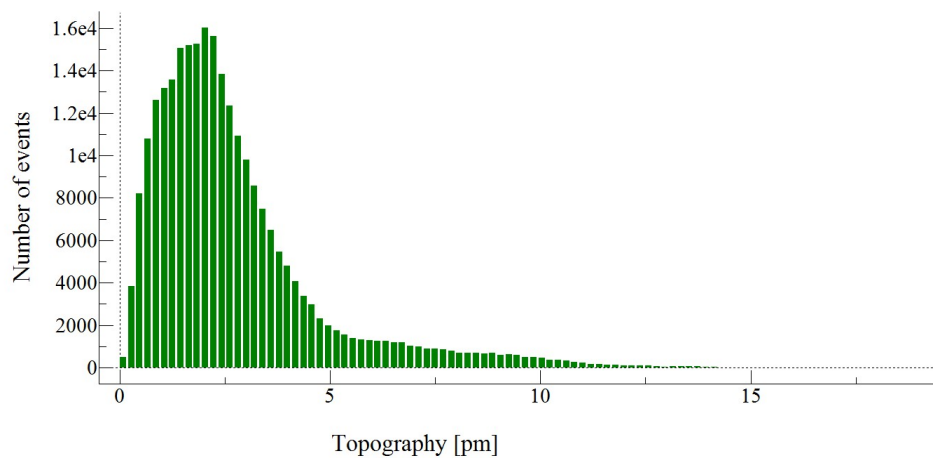**Figure 5.15:** Height distribution of Cu clusters+120+ozone+annealed

From the nanocluster height study it can be seen that there is a Gaussian distribution in the height of the clusters in a range from 5 nm until a little over 70 nm. In the range from 10 to 40 nm height most of the deposited nanoclusters were found.
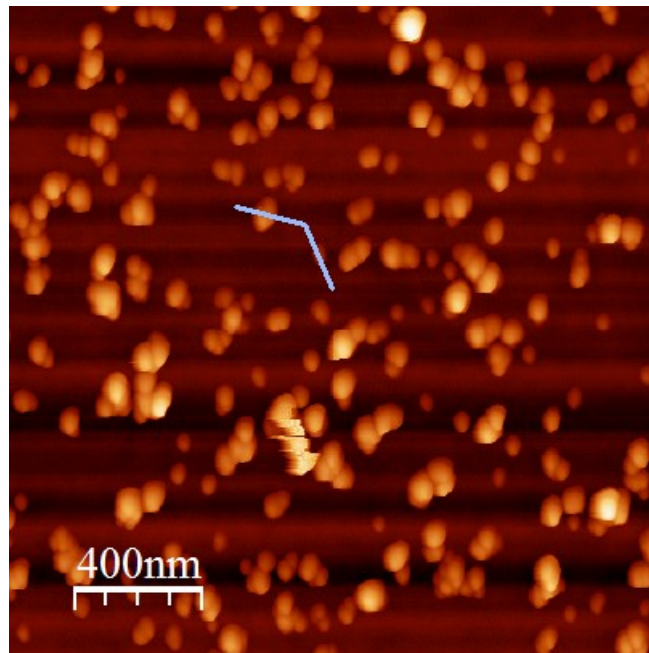

Figure 5.16: AFM image of Cu clusters+120+ozone+annealed+AgNP

The topographic image above shows a nice distribution of Cu clusters+120+Ozoned+annealed+AgNP. The distribution of the clusters is very dense and they seem to be deposited at different height from the PMMA surface. Here we can observe the formation of dimers, as we can see the particles into pairs. Hexanediol was used as a linker between the Cu cluster surface

and Colloidal AgNPs. As it can be seen in the below image, during the profile analysis one particle was measured to be at 35 nm height from the PMMA surface and one was measured to be at 10 nm height. It is evident that the bigger particle with 35 nm height is AgNP where as the one at 10 nm height is the Cu cluster.

Figure 5.17: Height analysis of Cu clusters+120+ozone+annealed+AgNP

Figure 5.18: Height distribution of Cu clusters+120+ozone+annealed+AgNP

From the nanocluster height study it can be seen that there is a Gaussian distribution in the height of the clusters in a range from 1 pm until a little over 15 pm. In the range from 2 to 5 pm height most of the deposited nanoclusters were found.

Figure 5.19: AFM image of Cu clusters+180

The topographic image above shows a nice distribution of Cu clusters+180. The distribution of the clusters is very dense and they seem to be deposited at different height from the PMMA surface. As it can be seen in the below image, during the profile analysis one particle was measured to be at 37 nm height from the PMMA surface and one was measured to be at 20 nm height.
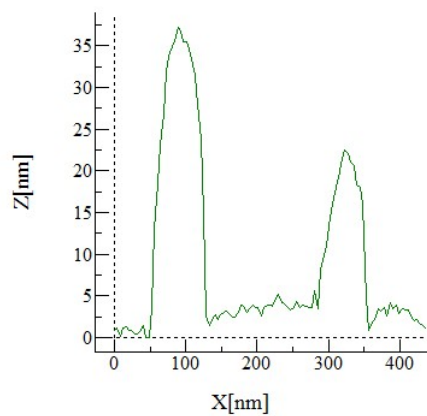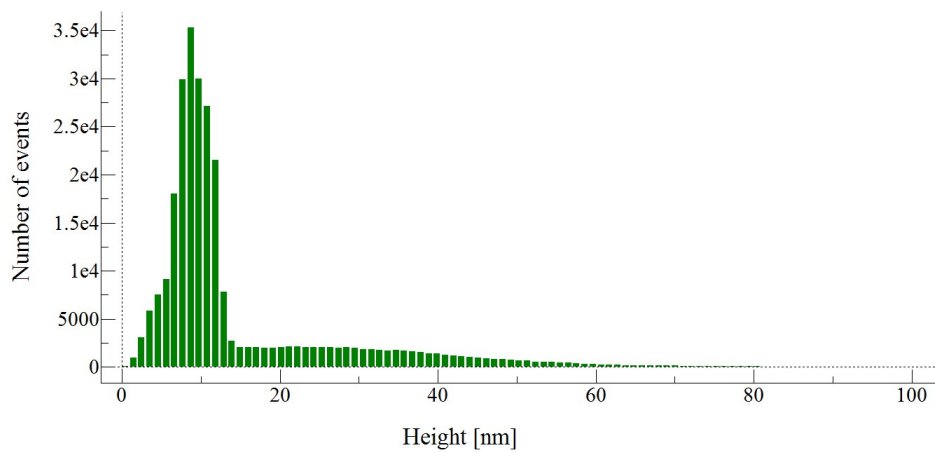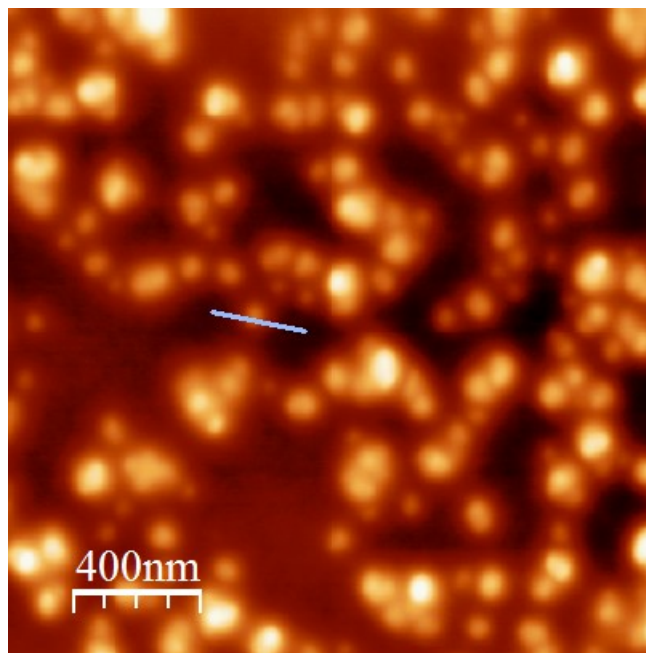

Figure 5.20: Height analysis of Cu clusters+180

Figure 5.21: Height distribution of Cu clusters+180

From the nanocluster height study it can be seen that there is a Gaussian distribution in the height of the clusters in a range from 4 nm until a little over 60 nm. In the range from 7 to 12 nm height most of the deposited nanoclusters were found.

Figure 5.22: AFM image of Cu clusters+180+ozone+annealed+AgNP

The topographic image above shows a nice distribution of Cu clusters+180+ozoned. The distribution of the clusters is very dense and they seem to be deposited at different height from the PMMA surface. Furthermore, the sample is observed after ozone treatment fro 30 min. Because of the ozone treatment, the particles appear to have formed a layer

surrounding them to prevent them from further oxidation. As it can be seen in the below image, during the profile analysis one particle was measured to be at 19 nm height from the PMMA surface.
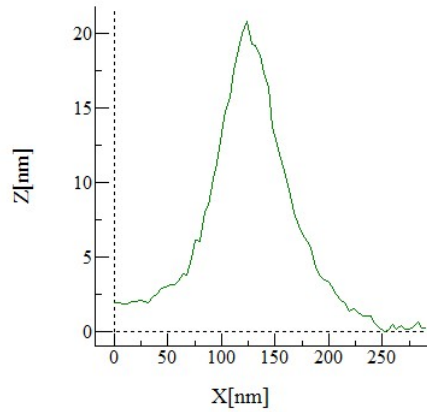

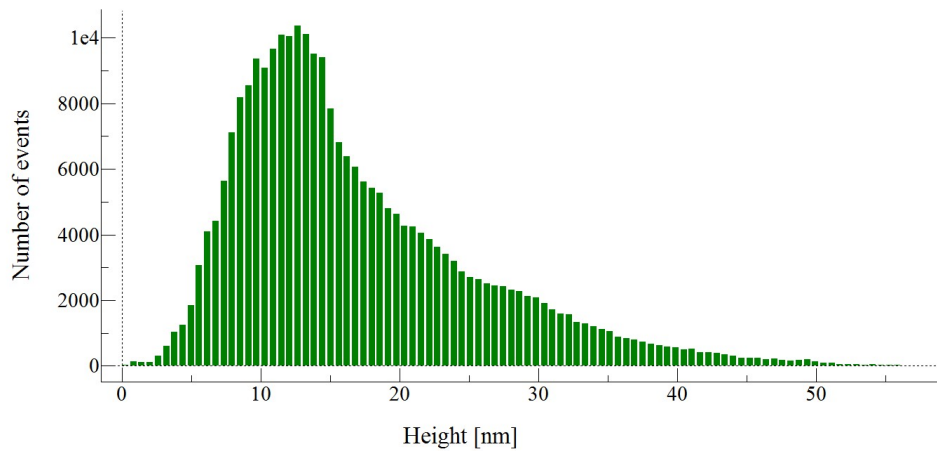**Figure 5.23:** Height analysis Cu clusters+180+ozone

Figure 5.24: Height distribution of Cu clusters+180+ozon

From the nanocluster height study it can be seen that there is a Gaussian distribution in the height of the clusters in a range from 5 nm until a little over 50 nm. In the range from 9 to 16 nm height most of the deposited nanoclusters were found.
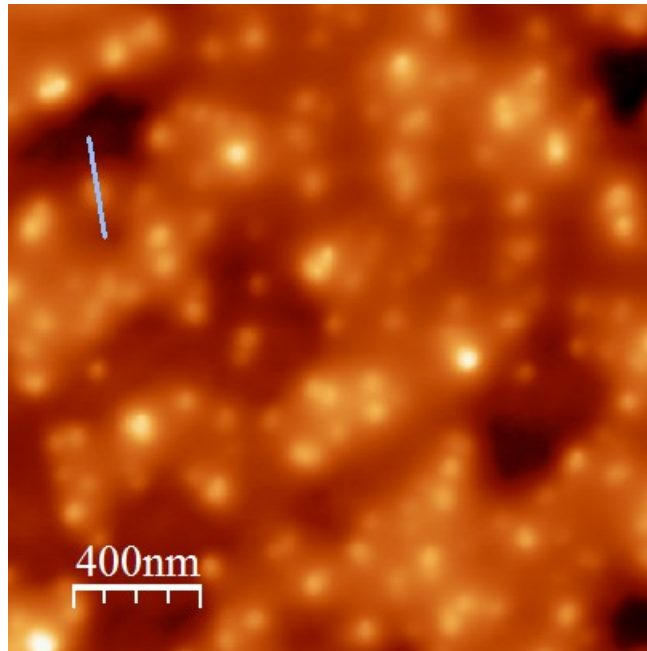
Figure 5.25: AFM image of Cu clusters+120+ozone+annealed

The topographic image above shows a nice distribution of Cu clusters+180+ozoned+annealed. The distribution of the clusters is very dense and they seem to be deposited at different height from the PMMA surface. The sample is after annealing process, so ideally some of the particles should get embedded into the PMMA and thus we expect the height analysis to show less height than the previous sample. As it can be seen in the below image, during the profile analysis one particle was measured to be 23 nm. The overall height distribution range was also observed to be decreased.
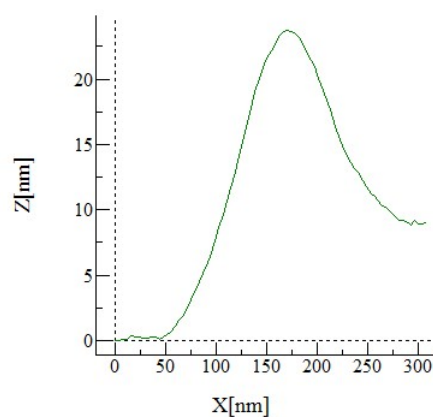

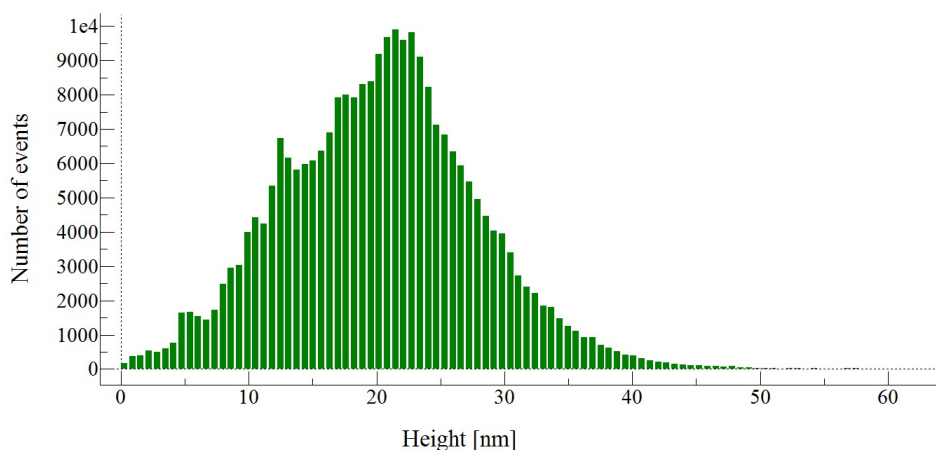**Figure 5.26:** Height analysis of Cu clusters+120+ozone+annealed

Figure 5.27: Height distribution of Cu clusters$_1$20$_o$zone$_a$nnealed

From the nanocluster height study it can be seen that there is a Gaussian distribution in the height of the clusters in a range from 2 nm until a little over 45 nm. In the range from 12 to 25 nm height most of the deposited nanoclusters were found.
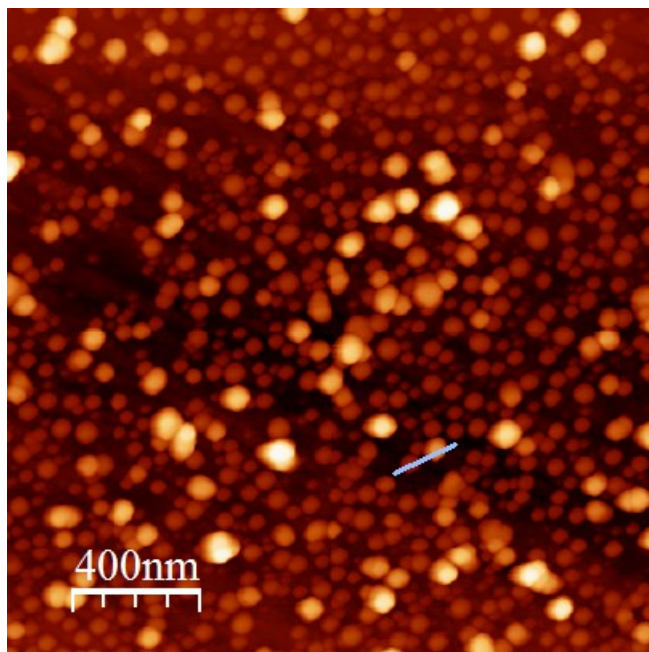

Figure 5.28: AFM image of Cu clusters+180+ozone+annealed+AgNP

The topographic image above shows a nice distribution of Cu clusters+180+Ozoned+annealed+AgNP. The distribution of the clusters is very dense and they seem to be deposited at different height from the PMMA surface. Here we can observe the formation of dimers, as we can see the particles into pairs. Hexanediol was used as a linker between the Cu cluster surface

and Colloidal AgNPs. As it can be seen in the below image, during the profile analysis one particle was measured to be at 25 nm height from the PMMA surface and one was measured to be at 10 nm height. It is evident that the bigger particle with 25 nm height is AgNP where as the one at 10 nm height is the Cu cluster.
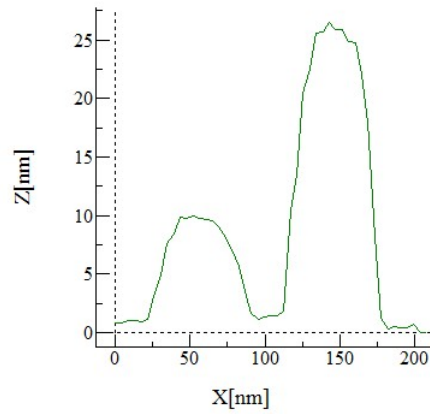

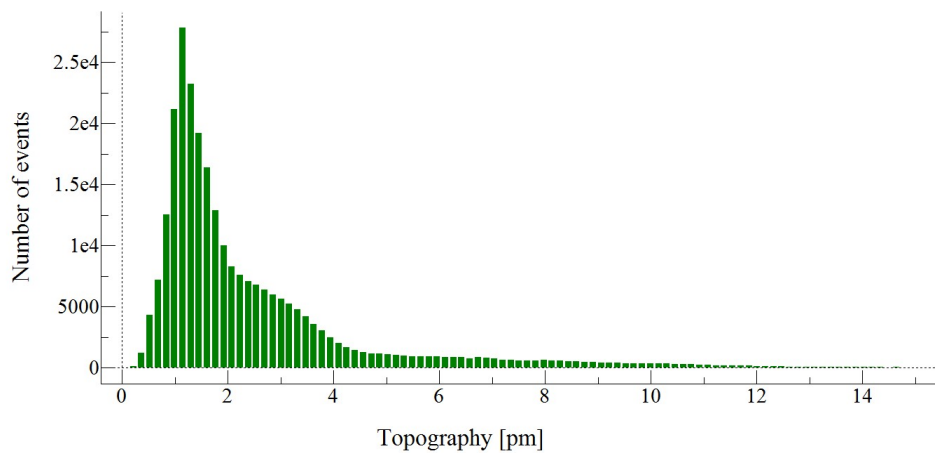**Figure 5.29:** Height analysis of Cu clusters+180+ozone+annealed+AgNP

Figure 5.30: Height distribution of Cu clusters+180+ozone+annealed+AgNP

From the nanocluster height study it can be seen that there is a Gaussian distribution in the height of the clusters in a range from 1 pm until a little over 10 pm. In the range from 2 to 4 pm height most of the deposited nanoclusters were found.

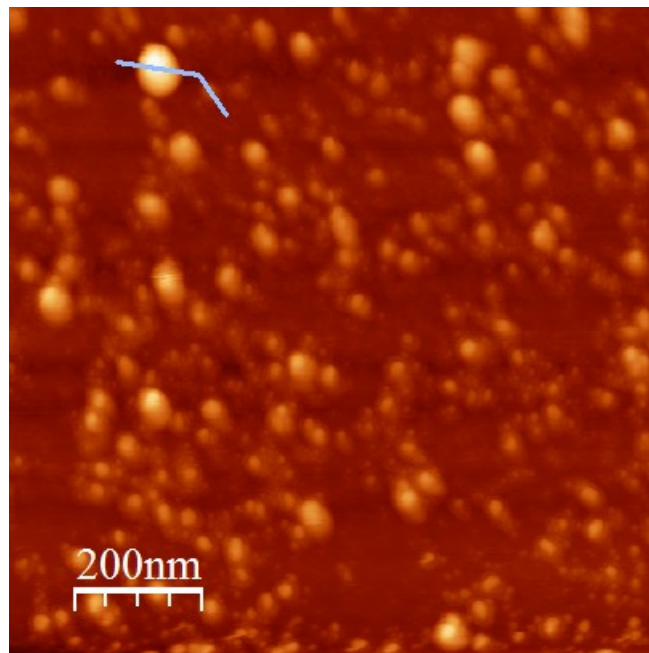## 5.5   AFM analysis of Ag Clusters+AgNP dimers

Figure 5.31: AFM image of Ag clusters+120

The topographic image above shows a nice distribution of Ag clusters+120. The distribution of the clusters is very dense and they seem to be deposited at different height from the PMMA surface. As it can be seen in the below image, during the profile analysis one particle was measured to be at 38 nm height from the PMMA surface and one was measured to be at 9 nm height.
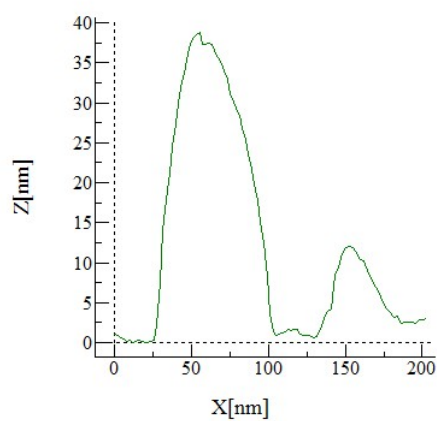

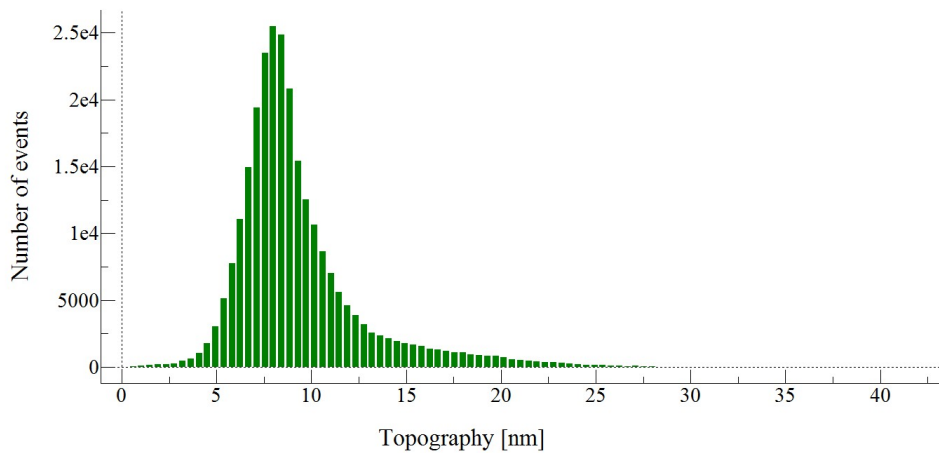**Figure 5.32:** Height analysis of AG clusters+120

Figure 5.33: Height distribution of AG clusters+120

From the nanocluster height study it can be seen that there is a Gaussian distribution in the height of the clusters in a range from 3 nm until a little over 25 nm. In the range from 7 to 13 nm height most of the deposited nanoclusters were found.

Figure 5.34: AFM image of AG clusters+120+annealed

The topographic image above shows a nice distribution of Ag clusters+120+annealed. The distribution of the clusters is very dense and they seem to be deposited at different height from the PMMA surface. The sample is after annealing process, so ideally some of the particles should get embedded into the PMMA and thus we expect the height analysis to

show less height than the previous sample. As it can be seen in the below image, during the profile analysis one particle was measured to be 10 nm and another at 6 nm. The overall height distribution range was observed to be decreased.

Figure 5.35: Height analysis of AG clusters+120+annealed

Figure 5.36: Height distribution of AG clusters+120+annealed

From the nanocluster height study it can be seen that there is a Gaussian distribution in the height of the clusters in a range from 1 nm until a little over 15 nm. In the range from 2 to 5 nm height most of the deposited nanoclusters were found.
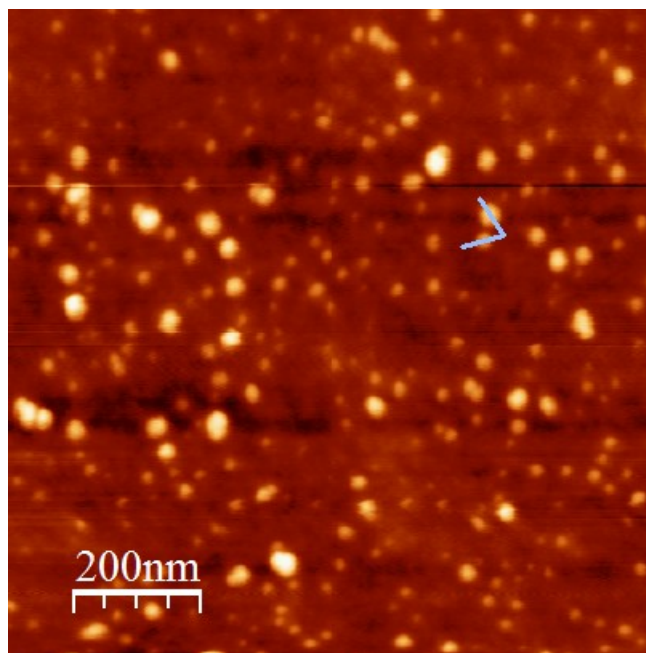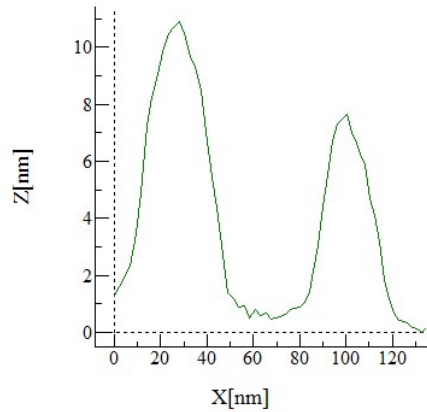
Figure 5.37: AFM image of AG clusters+120+annealed+AgNP

The topographic image above shows a nice distribution of Ag clusters+120+annealed+AgNP. The distribution of the clusters is very dense and they seem to be deposited at different height from the PMMA surface. Here we can observe the formation of dimers, as we can see the particles into pairs. Hexanediol was used as a linker between the Cu cluster surface and Colloidal AgNPs. As it can be seen in the below image, during the profile analysis one pair of the particles was measured to be at 12-14 nm height from the PMMA surface and one was measured to be at 5-6 nm height.
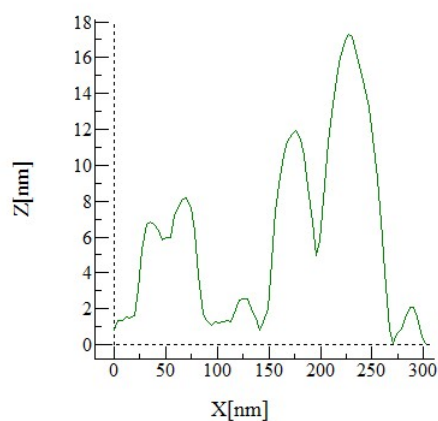
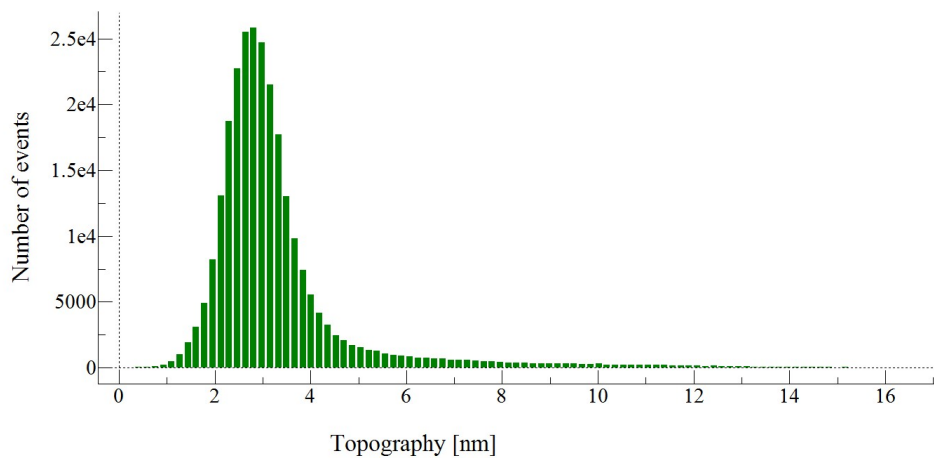**Figure 5.38:** Height analysis of AG clusters+120annealed+AgNP

Figure 5.39: Height distribution of AG clusters+120+annealed+AgNP

From the nanocluster height study it can be seen that there is a Gaussian distribution in the height of the clusters in a range from 3 nm until a little over 22 nm. In the range from 4 to 8 nm height most of the deposited nanoclusters were found.
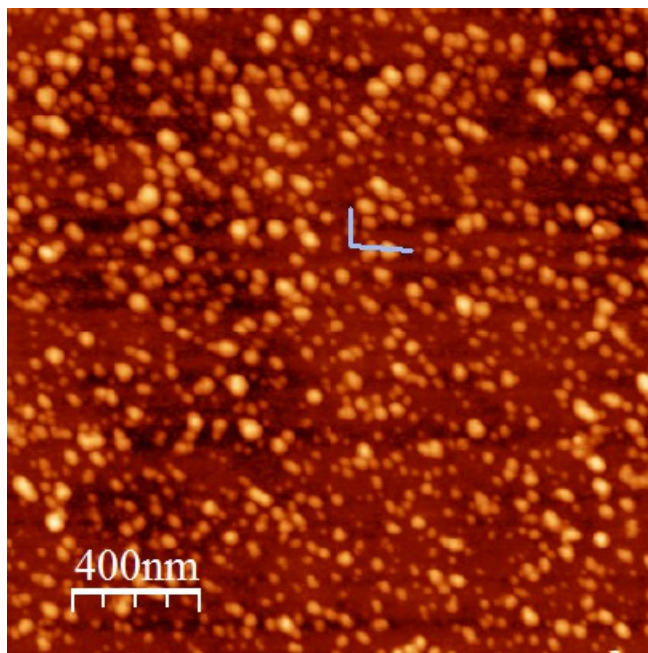

Figure 5.40: AFM image of AG clusters+180

The topographic image above shows a nice distribution of Ag clusters+180. The distribution of the clusters is very dense and they seem to be deposited at different height from the PMMA surface. As it can be seen in the below image, during the profile analysis one particle was measured to be at 12 nm height.
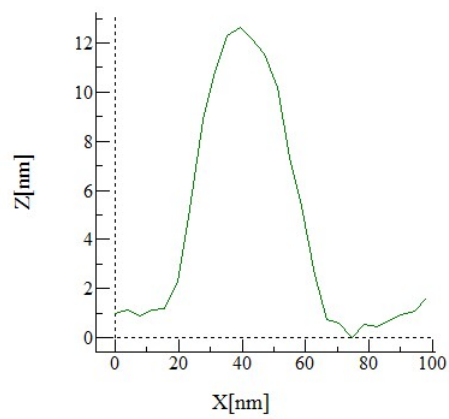
Figure 5.41: Height analysis of AG clusters+180

Figure 5.42: Height distribution of AG clusters+180

From the nanocluster height study it can be seen that there is a Gaussian distribution in the height of the clusters in a range from 3 nm until a little over 18 nm. In the range from 4 to 8 nm height most of the deposited nanoclusters were found.
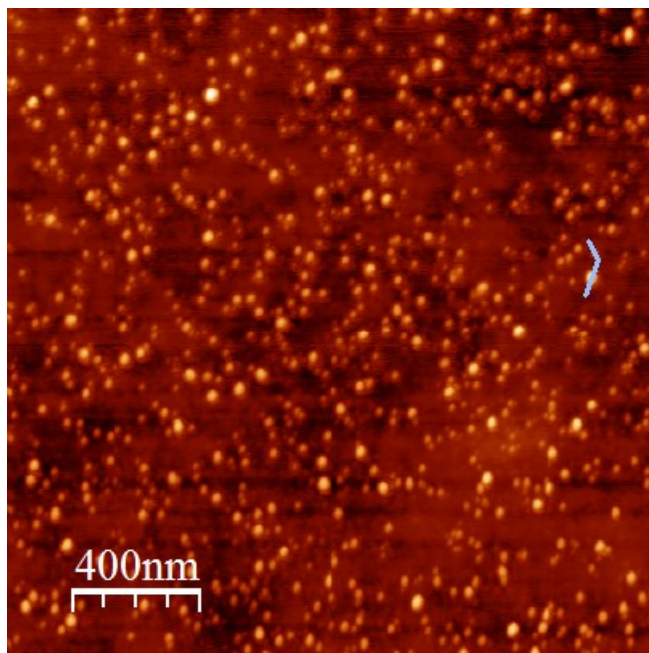
Figure 5.43: AFM image of AG clusters+180+annealed

The topographic image above shows a nice distribution of Ag clusters+180+annealed. The distribution of the clusters is very dense and they seem to be deposited at different height from the PMMA surface. The sample is after annealing process, so ideally some of the particles should get embedded into the PMMA and thus we expect the height analysis to show less height than the previous sample. As it can be seen in the below image, during the profile analysis one particle was measured to be 15 nm and one was measured to be at 7 nm height. SO some of the particles have been embedded into the PMMA. But the overall height distribution range was observed to be decreased.
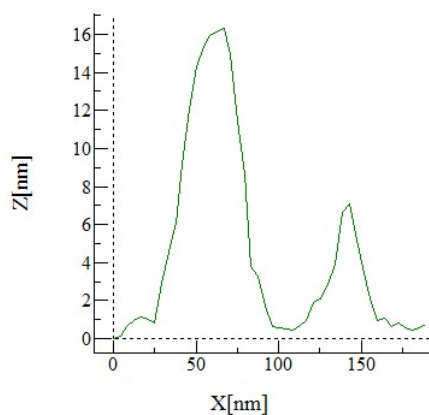
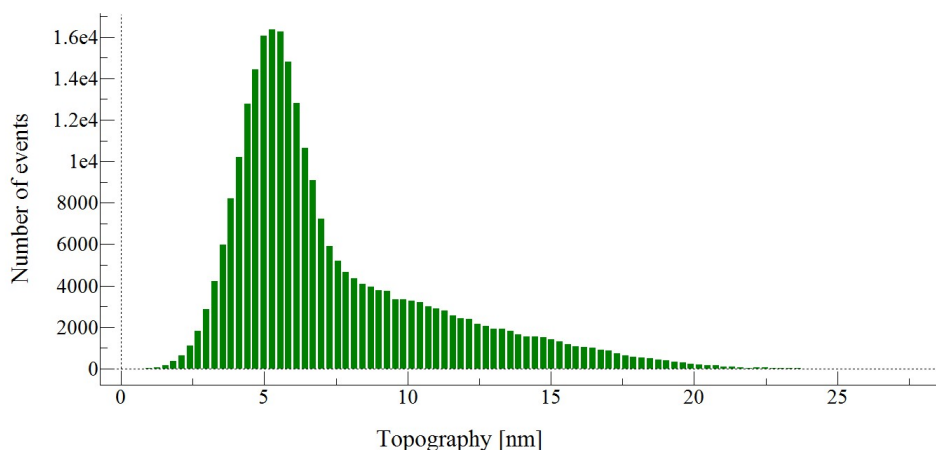**Figure 5.44:** Height analysis of AG clusters+180+annealed
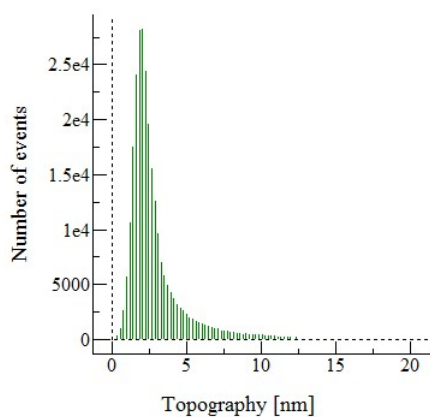
Figure 5.45: Height distribution of AG clusters+180+annealed

From the nanocluster height study it can be seen that there is a Gaussian distribution in the height of the clusters in a range from 2 nm until a little over 13 nm. In the range from 3 to 7 nm height most of the deposited nanoclusters were found.
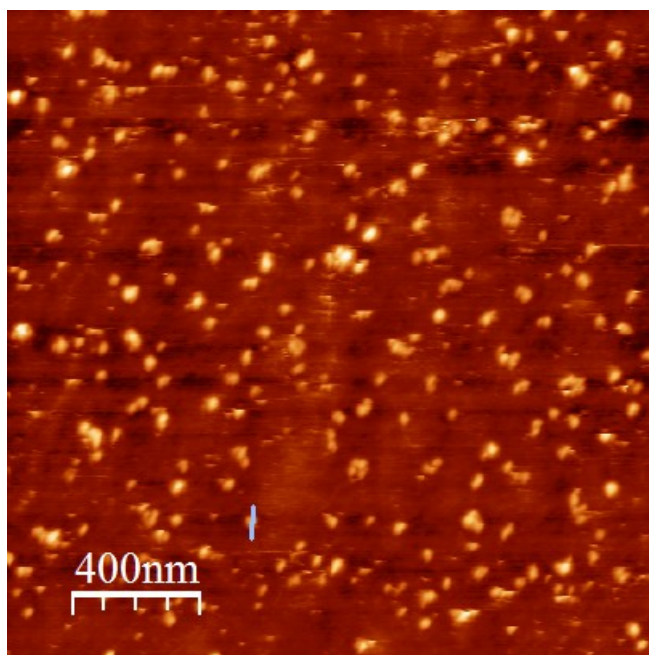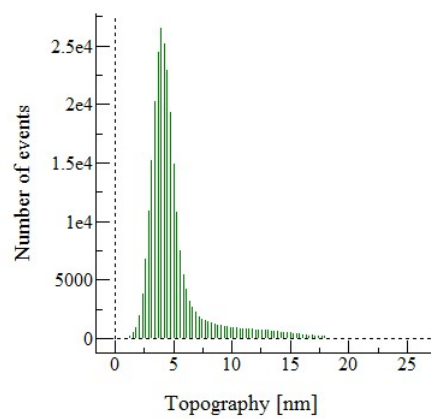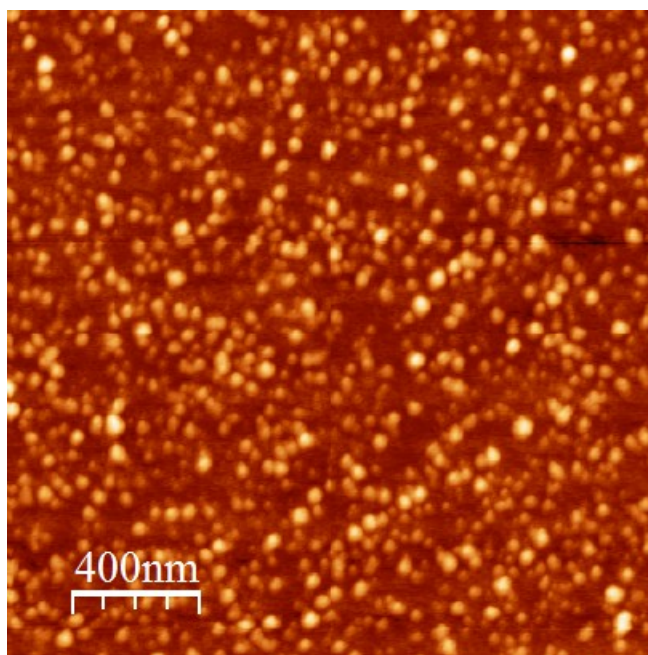

Figure 5.46: AFM image of AG clusters+180+annealed+AgNP

The topographic image above shows a nice distribution of Ag clusters+180+annealed+AgNP. The distribution of the clusters is very dense and they seem to be deposited at different height from the PMMA surface. Here we can observe the formation of dimers, as we can see the particles into pairs. Hexanediol was used as a linker between the Cu cluster surface and Colloidal AgNPs. As it can be seen in the below image, during the profile analysis

one pair of the particles was measured to be at 7-8 nm height from the PMMA surface and one was measured to be at 10-20 nm height. It is evident that the bigger particle with 10-20 nm height is AgNP where as the one at 7-8 nm height is the Ag cluster.
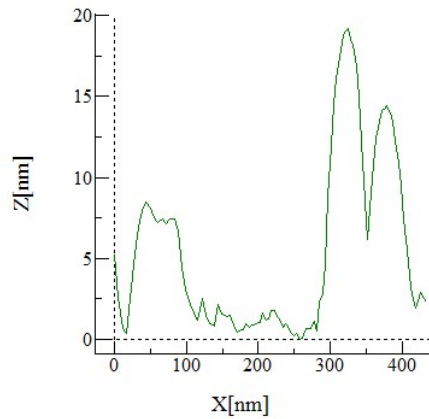
Figure 5.47: Height analysis of AG clusters+180+annealed+AgNP
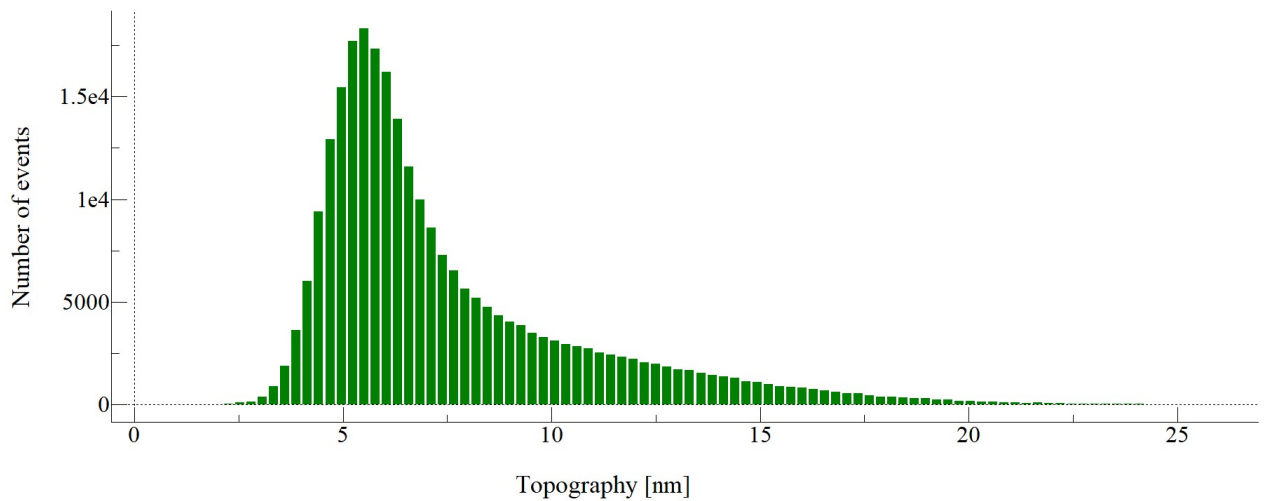
Figure 5.48: Height distribution of AG clusters+180+annealed+AgNP

From the nanocluster height study it can be seen that there is a Gaussian distribution in the height of the clusters in a range from 4 nm until a little over 20 nm. In the range from 5 to 9 nm height most of the deposited nanoclusters were found.

6. Conclusion

In this study, it has been proved possible to synthesize Nanoparticle dimers. The Copper clusters and Silver clusters were deposited on the PMMA coated quarts substrates (The PMMA coated quarts substrates were baked at 120 and 180 degree temperature.).Further the clusters were given ozone treatment and annealed.

Onto this annealed substrates, colloidal silver nanoparticles synthesized using citrate reduction method were loaded to prepare the nanoparticle dimers. 1-Hexanediol was used as a linker between the clusters and the colloidal particles.

Different characterization techniques were used to analyze the synthesized clusters, colloidal nanoparticles and the dimers and compared with each other.

UV visible NIR spectroscopy was used to measure the changes in spectra at different stages of processes like ozon treatment, annealing and after preparation of dimers.

Topography of the samples was studies using atomic force microscopy and height profiles and roughness analysis was performed to study the height distribution of the clusters and nanoparticles. It was observed that after the annealing, the clusters were partially embedded onto the PMMA surface.

NTA analysis was performed to analyze the size distribution of the colloidal silver nanoparticles.

Bibliography

[1] Gustav Mie. Beiträge zur optik trüber medien, speziell kolloidaler metallösungen. *Annalen der physik*, 330(3):377–445, 1908.

[2] Stephan Link and Mostafa A El-Sayed. Optical properties and ultrafast dynamics of metallic nanocrystals. *Annual review of physical chemistry*, 54(1):331–366, 2003.

[3] Prashant K Jain, Kyeong Seok Lee, Ivan H El-Sayed, and Mostafa A El-Sayed. Calculated absorption and scattering properties of gold nanoparticles of different size, shape, and composition: applications in biological imaging and biomedicine. *The journal of physical chemistry B*, 110(14):7238–7248, 2006.

[4] Jon P Camden, Jon A Dieringer, Yingmin Wang, David J Masiello, Lawrence D Marks, George C Schatz, and Richard P Van Duyne. Probing the structure of single-molecule surface-enhanced raman scattering hot spots. *Journal of the American Chemical Society*, 130(38):12616–12617, 2008.

[5] Samuel L Kleinman, Bhavya Sharma, Martin G Blaber, Anne-Isabelle Henry, Nicholas Valley, R Griffith Freeman, Michael J Natan, George C Schatz, and Richard P Van Duyne. Structure enhancement factor relationships in single gold nanoantennas by surface-enhanced raman excitation spectroscopy. *Journal of the American Chemical Society*, 135(1):301–308, 2012.

[6] Jeffrey M McMahon, Anne-Isabelle Henry, Kristin L Wustholz, Michael J Natan, R Griffith Freeman, Richard P Van Duyne, and George C Schatz. Gold nanoparticle dimer plasmonics: finite element method calculations of the electromagnetic enhancement to surface-enhanced raman spectroscopy. *Analytical and bioanalytical chemistry*, 394(7):1819–1825, 2009.

[7] J Britt Lassiter, Javier Aizpurua, Luis I Hernandez, Daniel W Brandl, Isabel Romero, Surbhi Lal, Jason H Hafner, Peter Nordlander, and Naomi J Halas. Close encounters between two nanoshells. *Nano letters*, 8(4):1212–1218, 2008.

[8] Duncan Graham, David G Thompson, W Ewen Smith, and Karen Faulds. Control of enhanced raman scattering using a dna-based assembly process of dye-coded nanoparticles. *Nature nanotechnology*, 3(9):548, 2008.

[9] M Homberger, S Schmid, J Timper, and U Simon. Solid phase supported "click"-chemistry approach for the preparation of water soluble gold nanoparticle dimers. *Journal of Cluster Science*, 23(4):1049–1059, 2012.

[10]   Xiaofeng Liu, Huibiao Liu, Weidong Zhou, Haiyan Zheng, Xiaodong Yin, Yuliang
       Li, Yanbing Guo, Mei Zhu, Canbin Ouyang, Daoben Zhu, et al. Thermoreversible
       covalent self-assembly of oligo (p-phenylenevinylene) bridged gold nanoparticles.
       Langmuir, 26(5):3179–3185, 2009.

[11]   Yulia Chaikin, Haim Leader, Ronit Popovitz-Biro, Alexander Vaskevich, and Israel
       Rubinstein. Versatile scheme for the step-by-step assembly of nanoparticle
       multilayers. *Langmuir*, 27(4):1298–1307, 2011.

[12]   Wyatt P McConnell, James P Novak, Louis C Brousseau, Ryan R Fuierer, Robert C
       Tenent, and Daniel L Feldheim. Electronic and optical properties of chemically
       modified metal nanoparticles and molecularly bridged nanoparticle arrays, 2000.

[13]   Marco P Stemmler, Yulia Fogel, Klaus Mullen, and Maximilian Kreiter. Bridging
       of gold nanoparticles by functional polyphenylene dendrimers. *Langmuir*,
       25(19):11917–11922, 2009.

[14]   Yaroslav A Urzhumov, Gennady Shvets, Jonathan Fan, Federico Capasso, Daniel
       Brandl, and Peter Nordlander. Plasmonic nanoclusters: a path towards
       negative-index metafluids. *Optics express*, 15(21):14129–14145, 2007.

[15]   Craig F Bohren and Donald R Huffman. *Absorption and scattering of light by small
       particles*. John Wiley & Sons, 2008.

[16]   Carsten Sönnichsen, Björn M Reinhard, Jan Liphardt, and A Paul Alivisatos. A
       molecular ruler based on plasmon coupling of single gold and silver nanoparticles.
       Nature biotechnology, 23(6):741, 2005.

[17]   Yon Ju-Nam and Jamie R Lead. Manufactured nanoparticles: an overview of their
       chemistry, interactions and potential environmental implications. *Science of the
       total environment*, 400(1-3):396–414, 2008.

[18]   Lorraine Mulfinger, Sally D Solomon, Mozghan Bahadory, Aravindan V
       Jeyarajasingam, Susan A Rutkowsky, and Charles Boritz. Synthesis and study of
       silver nanoparticles. *Journal of chemical education*, 84(2):322, 2007.

[19]   Isabel Pastoriza-Santos and Luis M Liz-Marzán. Reduction of silver nanoparticles
       in dmf. formation of monolayers and stable colloids. *Pure and Applied Chemistry*,
       72(1/2):83–90, 2000.

[20]   Rong He, Xuefeng Qian, Jie Yin, and Zikang Zhu. Preparation of polychrome silver
       nanoparticles in different solvents. *Journal of Materials Chemistry*,
       12(12):3783–3786, 2002.

[21]   Yugang Sun and Younan Xia. Shape-controlled synthesis of gold and silver
       nanoparticles. *Science*, 298(5601):2176–2179, 2002.

[22] Zeena S Pillai and Prashant V Kamat. What factors control the size and shape of silver nanoparticles in the citrate ion reduction method? *The Journal of Physical Chemistry B*, 108(3):945–951, 2004.

[23] EA Hernandez, B Posada, R Irizarry, and ME Castro. A new wet chemical approach for selective synthesis of silver nanowires. *NSTI-Nanotech 2004*, 3:156–158, 2004.

[24] Yu Lu, Gang L Liu, and Luke P Lee. High-density silver nanoparticle film with temperature-controllable interparticle spacing for a tunable surface enhanced raman scattering substrate. *Nano letters*, 5(1):5–9, 2005.

[25] Amit Sinha and BP Sharma. Preparation of silver powder through glycerol process. *Bulletin of Materials Science*, 28(3):213–217, 2005.

[26] Yadong Yin, Yu Lu, Yugang Sun, and Younan Xia. Silver nanowires can be directly coated with amorphous silica to generate well-controlled coaxial nanocables of silver/silica. *Nano Letters*, 2(4):427–430, 2002.

[27] Anjana Sarkar, Sudhir Kapoor, and Tulsi Mukherjee. Preparation, characterization, and surface modification of silver nanoparticles in formamide. *The Journal of Physical Chemistry B*, 109(16):7698–7704, 2005.

[28] A Graff, D Wagner, H Ditlbacher, and U Kreibig. Silver nanowires. *The European Physical Journal D-Atomic, Molecular, Optical and Plasma Physics*, 34(1-3):263–269, 2005.

[29] Kirti Patel, Sudhir Kapoor, D Purushotham Dave, and Tulsi Mukherjee. Synthesis of nanosized silver colloids by microwave dielectric heating. *Journal of Chemical Sciences*, 117(1):53–60, 2005.

[30] Asta Šileikaitė, Igoris Prosyčevas, Judita Puišo, Algimantas Juraitis, and Asta Guobienė. Analysis of silver nanoparticles produced by chemical reduction of silver salt solution. *Mater. Sci*, 12(4):1392–1320, 2006.

[31] Meng Chen, Li-Ying Wang, Jian-Tao Han, Jun-Yan Zhang, Zhi-Yuan Li, and Dong-Jin Qian. Preparation and study of polyacryamide-stabilized silver nanoparticles through a one-pot process. *The Journal of Physical Chemistry B*, 110(23):11224–11231, 2006.

[32] Chang Young Kim, Byung Moo Kim, Sung Hoon Jeong, and S Yi. Effect of sodium carbonate on the formation of colloidal silver particles by a reduction reaction of silver ions with pvp. *Journal of Ceramic Processing Research*, 7(3):241, 2006.

[33] B Viswanath, Paromita Kundu, B Mukherjee, and N Ravishankar. Predicting the growth of two-dimensional nanostructures. *Nanotechnology*, 19(19):195603, 2008.

[34] Chunhua Liu, Xiupei Yang, Hongyan Yuan, Zaide Zhou, and Dan Xiao. Preparation of silver nanoparticle and its application to the determination of ct-dna. *Sensors*, 7(5):708–718, 2007.

[35] M Raffi, Abdul K Rumaiz, MM Hasan, and S Ismat Shah. Studies of the growth parameters for silver nanoparticle synthesis by inert gas condensation. *Journal of Materials Research*, 22(12):3378–3384, 2007.

[36] Shun-Wen Wei, PENG Bing, Li-Yuan Chai, Yun-Chao Liu, and Zhu-Ying Li. Preparation of doping titania antibacterial powder by ultrasonic spray pyrolysis. *Transactions of Nonferrous Metals Society of China*, 18(5):1145–1150, 2008.

[37] Yongwen Zhang, Huashong Peng, Wei Huang, Yongfeng Zhou, Xuehong Zhang, and Deyue Yan. Hyperbranched poly (amidoamine) as the stabilizer and reductant to prepare colloid silver nanoparticles in situ and their antibacterial activity. *The Journal of Physical Chemistry C*, 112(7):2330–2336, 2008.

[38] Yongsoon Shin, In-Tae Bae, Bruce W Arey, and Gregory J Exarhos. Facile stabilization of gold-silver alloy nanoparticles on cellulose nanocrystal. *The Journal of Physical Chemistry C*, 112(13):4844–4848, 2008.

[39] Huabin Wang and Derek O Northwood. Synthesis of ag or pt nanoparticles by hydrolysis of either ag 2 na or ptna. *Advances in Materials Science and Engineering*, 2008, 2008.

[40] Lili Bo, Wu Yang, Miao Chen, Jinzhang Gao, and Qunji Xue. A simple and 'green'synthesis of polymer-based silver colloids and their antibacterial properties. *Chemistry & biodiversity*, 6(1):111–116, 2009.

[41] Yongsoon Shin, In-Tae Bae, and Gregory J Exarhos. "green" approach for self-assembly of platinum nanoparticles into nanowires in aqueous glucose solutions. *Colloids and Surfaces A: Physicochemical and Engineering Aspects*, 348(1-3):191–195, 2009.

[42] Pallab Sanpui, Shivendra B Pandey, Siddhartha Sankar Ghosh, and Arun Chattopadhyay. Green fluorescent protein for in situ synthesis of highly uniform au nanoparticles and monitoring protein denaturation. *Journal of colloid and interface science*, 326(1):129–137, 2008.

[43] Roberto Sato-Berrú, Rocío Redón, América Vázquez-Olmos, and José M Saniger. Silver nanoparticles synthesized by direct photoreduction of metal salts. application in surface-enhanced raman spectroscopy. *Journal of Raman Spectroscopy: An International Journal for Original Work in all Aspects of Raman Spectroscopy, Including Higher Order Processes, and also Brillouin and Rayleigh Scattering*, 40(4):376–380, 2009.

[44] Demberelnyamba Dorjnamjin, Maamaa Ariunaa, and Young Shim. Synthesis of silver nanoparticles using hydroxyl functionalized ionic liquids and their antimicrobial activity. *International journal of molecular sciences*, 9(5):807–820, 2008.

[45] R Das, SS Nath, D Chakdar, G Gope, and R Bhattacharjee. Preparation of silver nanoparticles and their characterization. *Journal of nanotechnology*, 5:1–6, 2009.

[46] Manjeet Singh, I Sinha, and RK Mandal. Role of ph in the green synthesis of silver nanoparticles. *Materials Letters*, 63(3-4):425–427, 2009.

[47] Dapeng Chen, Xueliang Qiao, Xiaolin Qiu, and Jianguo Chen. Synthesis and electrical properties of uniform silver nanoparticles for electronic applications. *Journal of materials science*, 44(4):1076–1081, 2009.

[48] Revathi Janardhanan, Murugan Karuppaiah, Neha Hebalkar, and Tata Narsinga Rao. Synthesis and surface chemistry of nano silver particles. *Polyhedron*, 28(12):2522–2530, 2009.

[49] Hyemin Choi, Bambang Veriansyah, Jaehoon Kim, Jae-Duck Kim, and Jeong Won Kang. Continuous synthesis of metal nanoparticles in supercritical methanol. *The Journal of Supercritical Fluids*, 52(3):285–291, 2010.

[50] Arnim Henglein. Colloidal silver nanoparticles: photochemical preparation and interaction with o2, ccl4, and some metal ions. *Chemistry of Materials*, 10(1):444–450, 1998.

[51] Nariaki Aihara, Kanjiro Torigoe, and Kunio Esumi. Preparation and characterization of gold and silver nanoparticles in layered laponite suspensions. *Langmuir*, 14(17):4945–4949, 1998.

[52] Abhijit Manna, Toyoko Imae, Masayasu Iida, and Naoko Hisamatsu. Formation of silver nanoparticles from a n-hexadecylethylenediamine silver nitrate complex. *Langmuir*, 17(19):6000–6004, 2001.

[53] Xue Zhang Lin, Xaowei Teng, and Hong Yang. Direct synthesis of narrowly dispersed silver nanoparticles using a single-source precursor. *Langmuir*, 19(24):10081–10085, 2003.

[54] Mathieu Maillard, Pinray Huang, and Louis Brus. Silver nanodisk growth by surface plasmon enhanced photoreduction of adsorbed [ag+]. *Nano Letters*, 3(11):1611–1615, 2003.

[55] MJ Rosemary and Thalappil Pradeep. Solvothermal synthesis of silver nanoparticles from thiolates. *Journal of colloid and interface science*, 268(1):81–84, 2003.

[56] Mark T Swihart. Vapor-phase synthesis of nanoparticles. *Current Opinion in Colloid & Interface Science*, 8(1):127–133, 2003.

[57] Yan Lu, Yu Mei, Marc Schrinner, Matthias Ballauff, Michael W Möller, and Josef Breu. In situ formation of ag nanoparticles in spherical polyacrylic acid brushes by uv irradiation. *The Journal of Physical Chemistry C*, 111(21):7676–7681, 2007.

[58] Jong-Seok Kim. Reduction of silver nitrate in ethanol by poly (n-vinylpyrrolidone). *Journal of Industrial and Engineering Chemistry*, 13(4):566–570, 2007.

[59] Yangying Chen and Xinkui Wang. Novel phase-transfer preparation of monodisperse silver and gold nanoparticles at room temperature. *Materials Letters*, 62(15):2215–2218, 2008.

[60] Jasmine A Jacob, Harbir S Mahal, Nandita Biswas, Tulsi Mukherjee, and Sudhir Kapoor. Role of phenol derivatives in the formation of silver nanoparticles. *Langmuir*, 24(2):528–533, 2008.

[61] T Maiyalagan. Synthesis, characterization and electrocatalytic activity of silver nanorods towards the reduction of benzyl chloride. *Applied Catalysis A: General*, 340(2):191–195, 2008.

[62] Luca Maretti, Paul S Billone, Yun Liu, and Juan C Scaiano. Facile photochemical synthesis and characterization of highly fluorescent silver nanoparticles. *Journal of the American Chemical Society*, 131(39):13972–13980, 2009.

[63] Abhishek P Kulkarni, Keiko Munechika, Kevin M Noone, Jessica M Smith, and David S Ginger. Phase transfer of large anisotropic plasmon resonant silver nanoparticles from aqueous to organic solution. *Langmuir*, 25(14):7932–7939, 2009.

[64] Assaf Ben Moshe and Gil Markovich. Synthesis of single crystal hollow silver nanoparticles in a fast reaction-diffusion process. *Chemistry of Materials*, 23(5):1239–1245, 2011.

[65] Xinyi Dong, Xiaohui Ji, Jing Jing, Mingyue Li, Jun Li, and Wensheng Yang. Synthesis of triangular silver nanoprisms by stepwise reduction of sodium borohydride and trisodium citrate. *The Journal of Physical Chemistry C*, 114(5):2070–2074, 2010.

[66] Dapeng Chen, Xueliang Qiao, Xiaolin Qiu, Jianguo Chen, and Renzhi Jiang. Large-scale synthesis of silver nanowires via a solvothermal method. *Journal of Materials Science: Materials in Electronics*, 22(1):6–13, 2011.

[67] Thabet M Tolaymat, Amro M El Badawy, Ash Genaidy, Kirk G Scheckel, Todd P Luxton, and Makram Suidan. An evidence-based environmental perspective of manufactured silver nanoparticle in syntheses and applications: a systematic review

and critical appraisal of peer-reviewed scientific papers. *Science of the total environment*, 408(5):999–1006, 2010.

[68] Arun Sudha, VS Murty, and TS Chandra. Standardization of metal-based herbal medicines. *Am J Infect Dis*, 5(3):193–199, 2009.

[69] Kaushik N Thakkar, Snehit S Mhatre, and Rasesh Y Parikh. Biological synthesis of metallic nanoparticles. *Nanomedicine: nanotechnology, biology and medicine*, 6(2):257–262, 2010.

[70] J García-Serna, L Pérez-Barrigón, and MJ Cocero. New trends for design towards sustainability in chemical engineering: Green engineering. *Chemical Engineering Journal*, 133(1-3):7–30, 2007.

[71] DC Tien, CY Liao, JC Huang, KH Tseng, JK Lung, TT Tsung, WS Kao, TH Tsai, TW Cheng, BS Yu, et al. Novel technique for preparing a nano-silver water suspension by the arc-discharge method. *Rev. Adv. Mater. Sci*, 18:750–756, 2008.

[72] Ki Tae Nam, Yun Jung Lee, Eric M Krauland, Stephen T Kottmann, and Angela M Belcher. Peptide-mediated reduction of silver ions on engineered biological scaffolds. *Acs Nano*, 2(7):1480–1486, 2008.

[73] Ramanathan Vaidyanathan, Kalimuthu Kalishwaralal, Shubaash Gopalram, and Sangiliyandi Gurunathan. Retracted: Nanosilver—the burgeoning therapeutic molecule and its green synthesis, 2009.

[74] Virender K Sharma, Ria A Yngard, and Yekaterina Lin. Silver nanoparticles: green synthesis and their antimicrobial activities. *Advances in colloid and interface science*, 145(1-2):83–96, 2009.

[75] Supin Sangsuk. Preparation of high surface area silver powder via tollens process under sonication. *Materials Letters*, 64(6):775–777, 2010.

[76] Bineta Keita, Guangjin Zhang, Anne Dolbecq, Pierre Mialane, Francis Sécheresse, Frédéric Miserque, and Louis Nadjo. Mov- movi mixed valence polyoxometalates for facile synthesis of stabilized metal nanoparticles: Electrocatalytic oxidation of alcohols. *The Journal of Physical Chemistry C*, 111(23):8145–8148, 2007.

[77] Nay Ming Huang, HN Lim, Shahidan Radiman, PS Khiew, WS Chiu, R Hashim, and Chin Hua Chia. Sucrose ester micellar-mediated synthesis of ag nanoparticles and the antibacterial properties. *Colloids and Surfaces A: Physicochemical and Engineering Aspects*, 353(1):69–76, 2010.

[78] A Safavi and S Zeinali. Synthesis of highly stable gold nanoparticles using conventional and geminal ionic liquids. *Colloids and Surfaces A: Physicochemical and Engineering Aspects*, 362(1-3):121–126, 2010.

[79]   Anh-Tuan Le, Phuong Dinh Tam, PT Huy, Tran Quang Huy, Nguyen Van Hieu, AA Kudrinskiy, Yu A Krutyakov, et al. Synthesis of oleic acid-stabilized silver nanoparticles and analysis of their antibacterial activity. *Materials Science and Engineering: C*, 30(6):910–916, 2010.

[80]   Fenghua Li, Fei Li, Jixia Song, Jiangfeng Song, Dongxue Han, and Li Niu. Green synthesis of highly stable platinum nanoparticles stabilized by amino-terminated ionic liquid and its electrocatalysts for dioxygen reduction and methanol oxidation. *Electrochemistry Communications*, 11(2):351–354, 2009.

[81]   Fabian Jutz, Jean-Michel Andanson, and Alfons Baiker. A green pathway for hydrogenations on ionic liquid-stabilized nanoparticles. *Journal of Catalysis*, 268(2):356–366, 2009.

[82]   Shelly Sinha, Ieshita Pan, Pompee Chanda, and Sukanta K Sen. Nanoparticles fabrication using ambient biological resources. *J Appl Biosci*, 19:1113–1130, 2009.

[83]   A Satyanarayana Reddy, Chien-Yen Chen, Simon C Baker, Chien-Cheng Chen, Jiin-Shuh Jean, Cheng-Wei Fan, Hau-Ren Chen, and Jung-Chen Wang. Synthesis of silver nanoparticles using surfactin: A biosurfactant as stabilizing agent. *Materials letters*, 63(15):1227–1230, 2009.

[84]   Yao-Chang Lee, Sin-Jia Chen, and Cheng-Liang Huang. Finding a facile method to synthesize decahedral silver nanoparticles through a systematic study of temperature effect on photomediated silver nanostructure growth. *Journal of the Chinese Chemical Society*, 57(3A):325–331, 2010.

[85]   YN Rao, D Banerjee, A Datta, SK Das, R Guin, and A Saha. Gamma irradiation route to synthesis of highly re-dispersible natural polymer capped silver nanoparticles. *Radiation Physics and Chemistry*, 79(12):1240–1246, 2010.

[86]   LM Cubillana-Aguilera, M Franco-Romano, MLA Gil, I Naranjo-Rodríguez, JL Hidalgo-Hidalgo De Cisneros, and JM Palacios-Santander. New, fast and green procedure for the synthesis of gold nanoparticles based on sonocatalysis. *Ultrasonics sonochemistry*, 18(3):789–794, 2011.

[87]   Nishat Arshi, Faheem Ahmed, MS Anwar, Shalendra Kumar, Bon Heun Koo, Junqing Lu, and Chan Gyu Lee. Novel and cost-effective synthesis of silver nanocrystals: a green synthesis. *Nano*, 6(04):295–300, 2011.

[88]   Kholoud MM Abou El-Nour, Ala'a Eftaiha, Abdulrhman Al-Warthan, and Reda AA Ammar. Synthesis and applications of silver nanoparticles. *Arabian journal of chemistry*, 3(3):135–140, 2010.

[89]   Liang-Shu Zhong, Jin-Song Hu, Zhi-Min Cui, Li-Jun Wan, and Wei-Guo Song. In-situ loading of noble metal nanoparticles on hydroxyl-group-rich titania

precursor and their catalytic applications. *Chemistry of Materials*,
19(18):4557–4562, 2007.

[90] Ziwei Deng, Min Chen, and Limin Wu. Novel method to fabricate sio2/ag
composite spheres and their catalytic, surface-enhanced raman scattering
properties. *The Journal of Physical Chemistry C*, 111(31):11692–11698, 2007.

[91] Xueping Jia, Xiaoyuan Ma, Dongwei Wei, Jian Dong, and Weiping Qian. Direct
formation of silver nanoparticles in cuttlebone-derived organic matrix for catalytic
applications. *Colloids and Surfaces A: Physicochemical and Engineering Aspects*,
330(2-3):234–240, 2008.

[92] M Bosetti, Alessandro Massè, E Tobin, and M Cannas. Silver coated materials for
external fixation devices: in vitro biocompatibility and genotoxicity. *Biomaterials*,
23(3):887–892, 2002.

[93] Min Cho, Hyenmi Chung, Wonyong Choi, and Jeyong Yoon. Different inactivation
behaviors of ms-2 phage and escherichia coli in tio2 photocatalytic disinfection.
Appl. Environ. Microbiol., 71(1):270–275, 2005.

[94] SL Percival, PG Bowler, and D Russell. Bacterial resistance to silver in wound
care. *Journal of hospital infection*, 60(1):1–7, 2005.

[95] Nelson Durán, Priscyla D Marcato, Gabriel IH De Souza, Oswaldo L Alves, and
Elisa Esposito. Antibacterial effect of silver nanoparticles produced by fungal
process on textile fabrics and their effluent treatment. *Journal of biomedical
nanotechnology*, 3(2):203–208, 2007.

[96] HJ Lee, Sang Young Yeo, and Sung Hoon Jeong. Antibacterial effect of nanosized
silver colloidal solution on textile fabrics. *Journal of Materials Science*,
38(10):2199–2204, 2003.

[97] Jong-in Hahm and Charles M Lieber. Direct ultrasensitive electrical detection of
dna and dna sequence variations using nanowire nanosensors. *Nano letters*,
4(1):51–54, 2004.

[98] JM Köhler, L Abahmane, J Wagner, J Albert, and G Mayer. Preparation of metal
nanoparticles with varied composition for catalytical applications in microreactors.
Chemical Engineering Science, 63(20):5048–5055, 2008.

[99] Miguel Pelaez, Nicholas T Nolan, Suresh C Pillai, Michael K Seery, Polycarpos
Falaras, Athanassios G Kontos, Patrick SM Dunlop, Jeremy WJ Hamilton,
J Anthony Byrne, Kevin O'shea, et al. A review on the visible light active titanium
dioxide photocatalysts for environmental applications. *Applied Catalysis B:
Environmental*, 125:331–349, 2012.

[100] Stéphane Berciaud, Laurent Cognet, Philippe Tamarat, and Brahim Lounis. Observation of intrinsic size effects in the optical response of individual gold nanoparticles. *Nano letters*, 5(3):515–518, 2005.

[101] Mostafa A El-Sayed. Some interesting properties of metals confined in time and nanometer space of different shapes. *Accounts of chemical research*, 34(4):257–264, 2001.

[102] Maryuri Roca, Nirajkumar H Pandya, Sudip Nath, and Amanda J Haes. Linear assembly of gold nanoparticle clusters via centrifugation. *Langmuir*, 26(3):2035–2041, 2009.

[103] C Jeffrey Brinker and George W Scherer. *Sol-gel science: the physics and chemistry of sol-gel processing.* Academic press, 2013.

[104] Jong-Won Park and Jennifer S Shumaker-Parry. Structural study of citrate layers on gold nanoparticles: role of intermolecular interactions in stabilizing nanoparticles. *Journal of the American Chemical Society*, 136(5):1907–1921, 2014.

[105] Željko Crljen, Predrag Lazić, Damir Šokčević, and Radovan Brako. Relaxation and reconstruction on (111) surfaces of au, pt, and cu. *Physical Review B*, 68(19):195411, 2003.

[106] Yongduo Liu and Vidvuds Ozolins. Self-assembled monolayers on au (111): structure, energetics, and mechanism of reconstruction lifting. *The Journal of Physical Chemistry C*, 116(7):4738–4747, 2012.

[107] M Mansfield and RJ Needs. Application of the frenkel-kontorova model to surface reconstructions. *Journal of Physics: Condensed Matter*, 2(10):2361, 1990.

[108] Randolph F Knarr, Roger A Quon, and T Kyle Vanderlick. Direct force measurements at the smooth gold/mica interface. *Langmuir*, 14(22):6414–6418, 1998.

[109] Norma A Alcantar, Chad Park, Jian-Mei Pan, and Jacob N Israelachvili. Adhesion and coalescence of ductile metal surfaces and nanoparticles. *Acta materialia*, 51(1):31–47, 2003.

[110] HBG Casimir and D Polder. The influence of retardation on the london-van der waals forces. *Physical Review*, 73(4):360, 1948.

[111] F Michael Serry, Dirk Walliser, and G Jordan Maclay. The anharmonic casimir oscillator (aco)-the casimir effect in a model microelectromechanical system. *Journal of Microelectromechanical Systems*, 4(4):193–205, 1995.

[112] Steven K Lamoreaux. Demonstration of the casimir force in the 0.6 to 6 μ m range. *Physical Review Letters*, 78(1):5, 1997.

[113] Jianping Zou, Z Marcet, Alejandro W Rodriguez, MT Homer Reid, AP McCauley, II Kravchenko, T Lu, Y Bao, SG Johnson, and HB Chan. Casimir forces on a silicon micromechanical chip. *Nature communications*, 4:1845, 2013.

[114] Evgenni Mikhailovich Lifshitz, M Hamermesh, et al. The theory of molecular attractive forces between solids. In *Perspectives in Theoretical Physics*, pages 329–349. Elsevier, 1992.

[115] Igor Ekhiel'evich Dzyaloshinskii, Efrat M Lifshitz, Lev P Pitaevskii, MG Priestley, et al. The general theory of van der waals forces. In *Perspectives in Theoretical Physics*, pages 443–492. Elsevier, 1992.

[116] Jeremy N Munday, Federico Capasso, and V Adrian Parsegian. Measured long-range repulsive casimir–lifshitz forces. *Nature*, 457(7226):170, 2009.

[117] Michael Grouchko, Polina Roitman, Xi Zhu, Inna Popov, Alexander Kamyshny, Haibin Su, and Shlomo Magdassi. Merging of metal nanoparticles driven by selective wettability of silver nanostructures. *Nature communications*, 5:2994, 2014.

[118] Cai Liu, Yong-Jun Li, Shi-Gang Sun, and Edward S Yeung. Room-temperature cold-welding of gold nanoparticles for enhancing the electrooxidation of carbon monoxide. *Chemical Communications*, 47(15):4481–4483, 2011.

[119] Gregory S Ferguson, Manoj K Chaudhury, George B Sigal, and George M Whitesides. Contact adhesion of thin gold films on elastomeric supports: cold welding under ambient conditions. *Science*, 253(5021):776–778, 1991.

[120] Richard J Cook, Heidi Fearn, and Peter W Milonni. Fizeau's experiment and the aharonov–bohm effect. *American Journal of Physics*, 63(8):705–710, 1995.

[121] Graham K Hubler. Pulsed laser deposition. *MRS Bulletin*, 17(2):26–29, 1992.

[122] Zhi-Ye Qiu, Cen Chen, Xiu-Mei Wang, and In-Seop Lee. Advances in the surface modification techniques of bone-related implants for last 10 years. *Regenerative biomaterials*, 1(1):67–79, 2014.

[123] E Yu Zykova, PA Karaseov, AI Titov, and VE Yurasova. Ion-surface interactions isi–2015. 2015.

[124] L Bardotti, B Prével, P Mélinon, Alejandra Perez, Q Hou, and M Hou. Deposition of au n clusters on au (111) surfaces. ii. experimental results and comparison with simulations. *Physical Review B*, 62(4):2835, 2000.

[125] Vladimir N Popok, Ingo Barke, Eleanor EB Campbell, and Karl-Heinz Meiwes-Broer. Cluster–surface interaction: From soft landing to implantation. *Surface Science Reports*, 66(10):347–377, 2011.

[126] Laurent Bardotti, Pablo Jensen, Alain Hoareau, Michel Treilleux, and Bernard Cabaud. Experimental observation of fast diffusion of large antimony clusters on graphite surfaces. *Physical review letters*, 74(23):4694, 1995.

[127] Pablo Jensen. Growth of nanostructures by cluster deposition: Experiments and simple models. *Reviews of Modern Physics*, 71(5):1695, 1999.

[128] B Prével, B Palpant, J Lermé, M Pellarin, M Treilleux, L Saviot, E Duval, A Perez, and M Broyer. Comparative analysis of optical properties of gold and silver clusters embedded in an alumina matrix. *NanoStructured Materials*, 12(1-4):307–310, 1999.

[129] Hans Dyrnesli, Gunnar Klös, Matteo Miola, and Duncan S Sutherland. Dynamic modulation of plasmonic structures. *Journal of Self-Assembly and Molecular Electronics (SAME)*, 7(1):1–22, 2019.